

Muonic hydrogen and the proton radius puzzle

RANDOLF POHL

Max-Planck-Institut für Quantenoptik, 85748 Garching, Germany

RONALD GILMAN

Department of Physics & Astronomy, Rutgers University, Piscataway, NJ

08854-8019, USA

GERALD A. MILLER

Department of Physics, Univ. of Washington, Seattle, WA 98195-1560, USA

KRZYSZTOF PACHUCKI

Faculty of Physics, University of Warsaw, Hoża 69, 00-681 Warsaw, Poland

Key Words Laser Spectroscopy, Atomic Physics, Proton Structure, Exotic
Atoms, Nuclear Physics, Lepton-Nucleon Scattering, QED, Beyond
the Standard Model

Abstract The extremely precise extraction of the proton radius by Pohl *et al.* from the measured energy difference between the 2P and 2S states of muonic hydrogen disagrees significantly with that extracted from electronic hydrogen or elastic electron-proton scattering. This is the proton radius puzzle. The origins of the puzzle and the reasons for believing it to be very significant are explained. Various possible solutions of the puzzle are identified, and future work needed to resolve the puzzle is discussed.

CONTENTS

Introduction	3
Electronic measurements	5
<i>Hydrogen spectroscopy</i>	5
<i>Elastic electron-proton scattering</i>	7
Measurement in muonic hydrogen	13
Potential solutions	16
<i>Muonic hydrogen experiment</i>	16
<i>Theory of muonic hydrogen</i>	17
<i>Proton Polarizability Effect in Muonic Hydrogen</i>	27
<i>Theory of hydrogen energy levels</i>	31
<i>Physics Beyond the Standard Model</i>	33
New projects	37
<i>New electron scattering experiments</i>	37
<i>Elastic muon-proton scattering</i>	39
<i>Spectroscopy of electronic atoms and ions</i>	41
<i>Spectroscopy of exotic atoms</i>	44
Conclusions	45
Acknowledgements	46

1 Introduction

The recent determination of the proton radius using the measurement of the Lamb shift in the muonic hydrogen atom [1, 2] startled the physics world. The obtained value of 0.84087(39) fm differs by about 4% or 7 standard deviations from the CODATA [3] value of 0.8775(51) fm. The latter is composed from the electronic hydrogenate atom value of 0.8758(77) fm and from a similar value with larger uncertainties determined by electron scattering [4]. The preceding sentence brings up a number of simple questions. The most prominent are: how can atomic physics be used to measure a fundamental property of a so-called elementary particle, why should muonic hydrogen be more sensitive to this quantity than electronic hydrogen, and why should a 4% difference between proton radii extracted using different techniques be important? In the present Introduction we sketch brief answers. The remainder of the article is devoted to detailed answers to these and related questions and implications.

The sensitivity of atomic energy levels to the non-zero size of the proton is determined by the probability that the bound lepton be within the volume of the proton. This probability is roughly given by the ratio of proton to atomic volumes: $(r_p/a_B)^3 = (\alpha m_r r_p)^3$, where r_p is the proton radius and m_r is the lepton reduced mass. The muon mass is about 200 times the electron mass so the muon is about 8 million more times likely to be inside the proton than the electron.

To be a bit more precise we need to define the proton radius. The mean-square value r_p^2 of the radius is given by

$$r_p^2 \equiv -6 \frac{dG_E}{dQ^2} \Big|_{Q^2=0}, \quad (1)$$

where G_E is the Sachs electric form factor of the proton and Q^2 is the negative of the square of the four-momentum transfer to the proton. We note in passing that, because of recoil effects, this radius is not actually the integral of r^2 times a true density [5,6]. However it is r_p^2 that is observable in energy levels of muon and electron hydrogen atoms.

For non-relativistic systems the lepton-proton Coulomb interaction is modified away from the point Coulomb interaction by the factor $G_E(Q^2)$ which is the probability amplitude for the proton to absorb the exchanged photon [7,8]. The resulting difference between the true potential and the potential for a point-like ($G_E = 1$) proton is given by

$$\delta V(\mathbf{r}) \equiv V_C(\mathbf{r}) - V_C^{\text{pt}}(\mathbf{r}) = -4\pi\alpha \int \frac{d^3q}{(2\pi)^3} \frac{(G_E(\mathbf{q}^2) - 1)}{\mathbf{q}^2} e^{-i\mathbf{q}\cdot\mathbf{r}}. \quad (2)$$

Using the expression $G_E(\mathbf{q}^2) - 1 \approx -\mathbf{q}^2 r_p^2 / 6$ in Eq. (2) is a very accurate approximation because in atomic physics $r_p q \sim r_p / a_B \sim 10^{-5}$. If this approximation is used, the perturbation δV is a Dirac-delta function at the origin multiplied by a factor that includes r_p , and the resulting energy shift for atomic S-states is given by [9]:

$$\Delta E = \langle \Psi_S | \delta V | \Psi_S \rangle = \frac{2}{3} \pi \alpha |\Psi_S(0)|^2 r_p^2. \quad (3)$$

The $S_{1/2}$ and $P_{1/2}$ states are degenerate for solutions of both the Schroedinger and Dirac equations. But with the effects of non-zero proton extent included, the $S_{1/2}$ state moves up and the $P_{1/2}$ state is not affected. This gives a contribution to the energy difference between $S_{1/2}$ and $P_{1/2}$ states, part of the Lamb shift.

The difference between the electronic and muonic determinations of the proton radius is very puzzling. One possibility is that experimental results are wrong. But multiple independent electron-proton experiments agree, and the muonic hy-

drogen experiment looks more convincing than any of the electron-proton experiments. Similarly, many measurements of transition frequencies in hydrogen are in agreement. As detailed in Sect. 2.1, the muonic hydrogen charge radius would require a change of the Rydberg constant [3] by 6.6 standard deviations [1, 2], in disagreement with the value obtained from many measurements in hydrogen. Another way out would be to assert that the various QED calculations that give contributions to the Lamb shift (other than the proton extent) are not sufficiently accurate. But all of the important contributions have been obtained by more than one group [7] and checked and rechecked. Another possibility is that the muon and electron have different interactions with the proton. But this violates a well-known and well-tested principle called lepton universality. The failure to understand why the proton radius can be different in muonic and electronic hydrogen is indeed a puzzle.

2 Electronic measurements

Fig. 1 shows several determinations of the proton charge radius. Early elastic electron-proton scattering measurements from Orsay [10], Stanford [11], Saskatoon [12, 13] and Mainz [14], and the various re-analyses of these world data [19, 23]. Spectroscopy of atomic hydrogen became sensitive to r_p on the percent level in the mid-1990s.

2.1 Hydrogen spectroscopy

Spectroscopy of atomic hydrogen (H) and deuterium (D) has been important the development of modern physics for more than a century. It was the discovery of the Lamb shift in H [24] which first showed effects of quantum electrodynamics

(QED) which go beyond the Dirac equation. Today, the 1S-2S transition in H has been measured with an accuracy of 4 parts in 10^{15} [25]. Other transitions, most notably the two-photon-transitions between the metastable 2S state and the states 8S,D [26] or 12D [27], have been measured with accuracies around 1 part in 10^{11} . For a review of the relevant transition frequencies in H and D see [3].

QED describes the energy levels of H with extraordinary accuracy. The test of QED using measured transition frequencies in H is limited by two of the input parameters required in the QED calculations, namely the Rydberg constant R_∞ and the rms proton charge radius r_p . Hence, one can either supply any of these two numbers from a source other than H spectroscopy (such as r_p from elastic e-p scattering of muonic hydrogen) and then test the correctness of QED, or use QED to extract the fundamental constants R_∞ and r_p .

Somewhat simplified, the energies of S-states in H are given by

$$E(nS) \simeq -\frac{R_\infty}{n^2} + \frac{L_{1S}}{n^3} \quad (4)$$

where n is the principal quantum number, and L_{1S} denotes the Lamb shift of the 1S ground state which is given by QED and contains the effect of the proton charge radius r_p . Numerically, $L_{1S} \simeq (8172 + 1.56 r_p^2)$ MHz when r_p is expressed in fm, so the finite size effect on the 1S level in H is about 1.2 MHz.

The different n -dependence of the two terms in Eq. (4) permits the determination of both R_∞ and r_p from at least two transition frequencies in H. Ideally, one uses the most accurately measured 1S-2S transition [25] and one of the 2S-8S,D/12D transitions [26, 27]. The former contains the maximal 1S Lamb shift L_{1S} and is hence maximally sensitive to r_p . The latter contain only smaller Lamb shift contributions due to the $1/n^3$ scaling in Eq. (4), and hence determine R_∞ . Fig. 2 shows the difference values of r_p obtained by combining the 1S-2S

transition and each of the other precisely measured transitions in H. In addition, it contains three values of r_p obtained from a direct measurement of the 2S-2P transitions in H. These are not sensitive to the Rydberg constant.

From Fig. 2 one can observe that all r_p values from H favor a larger r_p around 0.88 fm. Still, half of the individual r_p values agree with the muonic hydrogen value of 0.84 fm on the level of 1σ . In fact, only the 2S-8D_{5/2} transition [26] disagrees with the muonic r_p value on the level of 3σ . The discrepancy between the combined value from H, as obtained in the elaborate CODATA adjustment of the fundamental constants [3], and the muonic hydrogen value, is about 4.4σ .

2.2 Elastic electron-proton scattering

Elastic electron scattering has been used to measure the electromagnetic structure of nucleons and nuclei for about six decades, and been reviewed for nearly as long [28,29]. For the proton charge and magnetic radii, the key points are that the structure is encoded in two momentum-space, relativistic invariants – the electric and magnetic form factors $G_E(Q^2)$ and $G_M(Q^2)$ – and the radii are determined from the slope of the form factors at four-momentum transfer $Q^2 = 0$. (In this section the topic of the proton magnetic radius arises at times, but usually our remarks will be directed towards the charge radius.) In the one-photon exchange approximation, the measured experimental cross section is related to the form factors by

$$\frac{d\sigma}{d\Omega_{exp}} = \frac{d\sigma}{d\Omega_{point}} \times \left[\frac{G_E^2(Q^2) + \tau G_M^2(Q^2)}{1 + \tau} + 2\tau \tan^2(\theta/2) G_M^2(Q^2) \right]. \quad (5)$$

Here $\tau = Q^2/4m^2$ and θ is the lab scattering angle. Traditionally, cross section measurements were corrected for certain “radiative corrections”, higher order diagrams beyond the one-photon exchange approximation, not included in Eq. 5.

Form factors were extracted using Rosenbluth separations, multiple cross section measurements at different beam energies and scattering angles, resulting in the same momentum transfer. Then fits of the form factors with simple, sometimes theoretically inspired, parameterizations were used to determine the radii. However, due to a variety of issues with experiments and corrections, early radii extractions in the literature should no longer be taken seriously. One should instead be concerned with analyses of the past several years that pay attention to the issues mentioned below and are careful about extracting the radius.

Many of the issues in extracting a proton radius from scattering data have been known for over a decade [18,19]. These include

- The treatment of systematic uncertainties in many experiments was often unclear, and apparently optimistic. Fits to world data, taking the uncertainties as reported, do not give reduced χ^2 sufficiently close to 1.
- The radius determination is mainly sensitive to low Q^2 data, and world data fits can be satisfactory overall without going through the low Q^2 data.
- Fits extracting the radius using a single functional form typically ignored the uncertainty from model dependence.
- In principle the Taylor series expansion $G_E = 1 - Q^2 r_p^2/6 + Q^4 r_p^4/120 \dots$ gives a model independent radius determination. In practice the finite range of and uncertainties in the data lead to correlations between the coefficients r_p^n and possible truncation errors. Because the coefficients r_p^n grow with order, there is no Q^2 range where one term sufficiently dominates that its factor r_p^n can be fixed and used in fitting lower order terms to lower Q^2 data.

- Issues with the absolute normalization affect the extracted radius, but floating the normalization decreases sensitivity to the radius, and increases sensitivity to possible Q^2 dependent errors - the rapid change of the cross section and data rates with Q^2 is a problem.
- Early radius extractions lacked Coulomb corrections, the acceleration of the electron in the proton's Coulomb field, which tend to increase the extracted radius about 0.01 fm [18].

The observation of differences in the ratio $G_E(Q^2)/G_M(Q^2)$ measured by Rosenbluth techniques and by polarization transfer techniques, first observed in [30] ultimately led to the recognition of the importance of hard two-photon exchange corrections [31], ignored in earlier work. Calculations of two-photon exchange depend on the off-shell structure of the proton, and are not under precise theoretical control. Experimental measurements generally constrained two-photon effects to be no more than $\approx 1\%$. This topic continues to be under active investigation, due to its potential impact on knowledge of the proton structure, and of the radius. High precision experiments are under way to determine observables that depend on two-photon exchange, such as difference in e^+p and e^-p cross sections, single spin asymmetries, and variations in form factor ratios extracted at the same momentum transfer as a function of the beam energy or scattering angle. While two-photon exchange should be under better control in the near future, it is currently believed to be a small correction for low Q^2 data of most importance to the radius puzzle, and mainly of importance in determining the magnetic radius [32].

A renewed interest in the long-range, low- Q^2 structure of the proton led to several new electron scattering experiments performed at the same time as the

muonic hydrogen experiment. The Bates BLAST collaboration [33] used a polarized electron beam incident on a polarized gas target to determine that the form factor ratio $\mu G_E/G_M$ was close to unity for $Q^2 \approx 0.15 \rightarrow 0.6 \text{ GeV}^2$. The Jefferson Lab LEDEX collaboration [34,35] used polarization transfer to determine that the form factor ratio deviated significantly from unity by $0.3 - 0.4 \text{ GeV}^2$, subsequently confirmed and improved upon in [15]. Note that while the polarization data give a form factor ratio, which does not determine the radius, the ratio does help constrain normalizations of cross section data during fits, leading to an improved value of the radius. The analysis of [15] gives confirms the larger proton radius of electron measurements, $r_p = 0.875 \pm 0.008_{exp} \pm 0.006_{fit}$. Data that extend the form factor ratios to even lower Q^2 , $0.01 \text{ GeV}^2 - 0.06 \text{ GeV}^2$ are currently under analysis [36].

Most importantly for the radius puzzle, the Mainz A1 collaboration [4] measured 1422 precise relative cross sections over a wide range of angles ($20^\circ - 135^\circ$) and beam energies (180 MeV - 855 MeV), corresponding to $Q^2 = 0.0038 \rightarrow 0.98 \text{ GeV}^2$. Experimental systematic uncertainties were controlled by using one spectrometer as a luminosity monitor, and by determining cross sections with two spectrometers moved through multiple, overlapping angle settings. The data were fit with a variety of functional forms using 31 normalization constants. Generally it was found that a good $\chi^2/\text{d.o.f.}$, ≈ 1.14 , could be obtained with flexible forms (polynomials or splines) but not with inflexible forms, such as dipoles. Polynomials and splines led to slightly different extracted radii, leading to $r_p = 0.879 \pm 0.005_{stat} \pm 0.004_{syst} \pm 0.002_{model} \pm 0.004_{group}$, where the final uncertainty comes from the polynomial vs. spline difference.

The fits of [4] and [15] use entirely independent data sets, and give form factor

ratios in good agreement in the more limited Q^2 range of the polarization data [15]. The proton charge radii from the two fits also agree, but the magnetic radii are significantly different. A large part of the difference appears to result from different treatments of the two-photon exchange corrections [37, 38], and it appears that the difference in magnetic radii has no effect on the determination of the electric radius.

These new experimental reports reinforce the proton radius puzzle. Several independent analyses of the proton radius have also been made. Here we highlight four recent contradictory results.

Dispersion relations and the vector meson dominance model have long been used to fit the form factors, with the space-like form factors resulting from poles in the time-like region. Various other features such as continuum contributions and expected high- Q^2 asymptotic behavior have been added. The most recent work of this sort [39] finds $r_p = 0.84 \pm 0.01$ fm with $\chi^2/\text{d.o.f} \approx 2.2$. Several notes are in order. Neutron and proton data are simultaneously fit. The Mainz A1 data set normalization is allowed to float, and in most cases the change is less than 1%. Statistically, the reduced χ^2 of 2.2 indicates that the data are not well described by the fit; while in general this could result from underestimated uncertainties in the data, the lower χ^2 of the flexible fits of [4, 40] suggest this is not the case here. However, visually the fits of [39] go through all the lower Q^2 data well, and start to diverge somewhat at larger values of Q^2 . This suggests that for determining the radius the large value of χ^2 is not an issue, but that there may be an issue with inappropriate strength in higher order terms – thinking in terms of the Taylor series expansion – leading to an incorrect result for the radius term. The smaller charge radius in these dispersion relation fits is in line with

previous fits of this type [17, 41].

The z expansion – see [42] for its application to the proton form factors – provides a method of incorporating physical constraints (analyticity) in choosing a functional form to fit the form factor data. The form factor is parameterized as a power series in a complex variable $z(Q^2)$ that is constrained to lie within the unit circle. The power series expansion of the form factor is model independent, unlike the particular functional forms chosen in the dispersion relations analyses of [17, 39, 41] and others. The benefits of this transformation include a maximum value of z and coefficients that are bounded, guaranteeing a finite number of terms will be adequate. A fit with only the proton data yields $r_p = 0.870 \text{ fm} \pm 0.023 \text{ fm} \pm 0.012 \text{ fm}$; while including neutron data and the $\pi\pi$ continuum leads to $r_p = 0.871 \text{ fm} \pm 0.009 \text{ fm} \pm 0.002 \text{ fm} \pm 0.002 \text{ fm}$ - see [42] for details. While the analysis continues to suggest a larger proton radius, it also suggests that the proton radius uncertainties are underestimated by other recent analyses.

Some of the issues discussed previously in relation to fits were revisited in recent work by Sick [43, 44]. The extraction of the proton radius was found to be most sensitive to data in the range $0.01 \text{ GeV}^2 \rightarrow 0.06 \text{ GeV}^2$ ($0.5 \text{ fm}^{-1} \rightarrow 1.3 \text{ fm}^{-1}$). Fit functions with polynomials in a denominator can, with negative terms in the denominator, generate pathological behaviors – poles in the form factors at high Q^2 outside the range of data. Thinking in terms of the Fourier transform of a spatial distribution, this generates non-physical oscillatory behavior that extends to large r and affects the radius extracted. Despite the low Q^2 of the Mainz data, fits of the data would be more reliable if the data extended to lower Q^2 and / or did not have a floating normalization. Parameterizations that correspond to a more sensible large r fall off should be safer. A sum-of-Gaussians r -space fit gave

a stable radius determination, without the issues discussed, of $r_p = 0.886 \text{ fm} \pm 0.008 \text{ fm}$.

Recent unpublished work by C.E. Carlson and K. Griffioen points out that a linear fit to the lowest Q^2 Mainz data, $Q^2 < 0.02 \text{ GeV}^2$, where G_E appears to be entirely linear, yields $r_p \approx 0.84 \text{ fm}$, rather than $\approx 0.88 \text{ fm}$. But great care must be taken in doing any such fit [19]. Since for the proton $r_p^4 > 0$, the quadratic term in the Taylor series expansion nearly guarantees that a linear fit to low Q^2 data will underestimate the radius. An estimate of the potential size of the effect can be made with the Kelly form factor parameterization [45], which has $r_p \approx 0.86 \text{ fm}$. A fit to pseudodata up to 0.02 GeV^2 , with the density and statistics of the Mainz data set, yields $r_p \approx 0.84 \text{ fm} \pm 0.01 \text{ fm}$. Adding in a quadratic term leads to uncertainties on r_p too large to distinguish between 0.84 fm and 0.88 fm . Similar concerns apply to an extension of this approach up to 0.2 GeV^2 . An extensive study of this issue has been performed by M.O. Distler.

To summarize, the apparently simple problem of determining the slope of the form factor at $Q^2 = 0$ has numerous potential pitfalls. The weight of the evidence at this point continues to favor a larger radius, about 0.88 fm , but suggests that claiming an uncertainty at the 0.01 fm level is optimistic.

3 Measurement in muonic hydrogen

A measurement of the Lamb shift in muonic hydrogen (μp) was initially considered half a century ago as a test of electron vacuum polarization effects [46], complementary to the Lamb shift in regular, electronic hydrogen [24] which is dominated by the electron self-energy [47]. The first observation of x-rays from muonic hydrogen succeeded shortly afterwards [48].

Laser spectroscopy of the 2S-2P transition in μp requires, however, μp atoms in the metastable 2S state. Several groups failed to observe such long-lived $\mu\text{p}(2\text{S})$ atoms when muons are stopped in molecular hydrogen gas [49–52], see also [53]. The first observation of long-lived μp atoms in the 2S state [54–56] was the starting point [57–59] of the recent Lamb shift measurement [1, 2].

When negative muons are stopped in molecular H_2 gas at low pressure (1 mbar at room temperature), about 1% of the muons form $\mu\text{p}(2\text{S})$ atoms [54, 60] with a lifetime of about $1\,\mu\text{s}$ [56]. At higher gas pressures the 2S state is quickly de-excited in collisions with H_2 molecules.

A novel beam line for low-energy negative muons [59] was built at Paul-Scherrer-Institute (PSI) in Switzerland which delivers about 600 μ^- per second with a kinetic energy between 3 keV and 6 keV. About half of the muons stop in 1 mbar H_2 gas within a target vessel which has a length of 20 cm along the muon beam axis. The transverse dimensions of the muon beam are $0.5 \times 1.5\,\text{cm}^2$. Hence the muon stop volume is small enough to be illuminated with laser light of sufficiently high fluence (see below). The muons arrive at random times, so each muon has to be detected before it enters the target vessel. Two stacks of ultra-thin carbon foils, separated by $\sim 35\,\text{cm}$, are used to detect the muon with high efficiency (80% and 70%, respectively) using secondary electrons ejected by muons crossing the carbon foils. A signal in both carbon foil stacks, with the correct time-of-flight for a low-energy muon traveling the distance between the carbon stacks, serves as a start signal for the data acquisition and the pulsed laser system.

The pulsed laser system [61, 62] delivers 5 ns long pulses of light with a wavelength tunable from $5.5\,\mu\text{m}$ to $6.1\,\mu\text{m}$, with a pulse energy of about 0.25 mJ. A

cw-pumped Yb:YAG disk laser system [62, 63] produces 100 mJ of pulsed pump light only a few hundred nanoseconds after a muon-induced trigger signal at a random time. This light is used to amplify red light, tunable around 708 nm, using Ti:sapphire crystals. The red pulses are converted to the desired infrared (IR) wavelength at 5.5-6 μm via three sequential Stokes shifts in a high-pressure Raman cell [64]. The frequency of the laser light is stabilized and controlled at 708 nm, and calibrated in the IR using well-known absorption lines of water vapor (H_2O). These H_2O lines are known with an accuracy of a few MHz, but pulse-to-pulse energy fluctuations of the laser system cause a broadening of the laser line width resulting in the final 300 MHz uncertainty of the laser frequency calibration [1].

A non-resonant multi-pass mirror cavity [65] inside the target gas vessel ensures efficient illumination of the muon stop volume inside the H_2 target gas. The estimated laser fluence is about 6 mJ/cm², which results in approximately 30% transition probability when the laser is tuned to the center of the resonance.

The successful 2S-2P laser excitation is signaled by the emission of a 1.9 keV K_α x-ray which is emitted in the radiative 2P-1S de-excitation that follows the 2S-2P transition immediately. The x-rays are detected in 20 large-area avalanche photo diodes (LAAPDs, $14 \times 14 \text{ mm}^2$ active area each) [66, 67] which are mounted close to the muon stop volume.

The experiment [1, 2] records time spectra of K_α x-rays for various laser frequencies (i.e. wavelengths) [68]. For each time spectrum, the number of K_α x-rays in the time window at which the laser illuminates the muon stop volume is normalized by the “prompt” K_α x-rays which are emitted by the 99% of the muons which do not populate the metastable 2S state, but proceed directly to the 1S

ground state.

The resonance curve in Fig. 3 is obtained by plotting the normalized number of laser-induced K_α x-rays as a function of laser frequency. The fit of this resonance curve reveals the resonance frequency and hence the Lamb shift in muonic hydrogen [1, 2].

4 Potential solutions

The various possible explanations of the proton radius puzzle are discussed in this section.

4.1 Muonic hydrogen experiment

The discrepancy between the observed resonance position in muonic hydrogen [1, 2] and the predictions using the r_p values from elastic electron scattering [19, 23] or hydrogen spectroscopy [22] (which together form the CODATA values 2006 and 2010) is enormous, as can be seen in Fig. 3.

The resonance center is 75 GHz away from the central value of the CODATA prediction. This corresponds to about four times the width of the resonance. The statistical uncertainty of the resonance center is about 700 MHz, i.e. 1/100 of the discrepancy. The systematic uncertainty of the measurement is 300 MHz. It is due to the laser frequency calibration mentioned in Sect. 3. Other systematic effects like ac- and dc-Stark shifts, Zeeman shifts, Doppler shifts etc. have been investigated but were found to be even smaller [1].

It is obvious from these numbers that the discrepancy is severe, and it is difficult to imagine an effect that could shift the resonance position by 4 line widths. Jentschura [69] found that the presence of an electron could result in a shift of

the resonance position if the distance between the electron and the $\mu\text{p}(2\text{S})$ atom was about 1 (electronic) Bohr radius. He suggested that the spectroscopy might have happened not on a $\mu\text{p}(2\text{S})$ atom, but on the molecular ion $p\mu e^-$.

Karr and Hilico [70] studied the 3-body systems $p\mu e^-$ and $pp\mu^-$ and found that these are not stable. In addition, the molecular ion $pp\mu^-$ has been calculated to be very short-lived [71–73]. The observation of the quenching of long-lived $\mu\text{p}(2\text{S})$ atoms [56] supports this picture. Hence, the proton radius puzzle cannot be explained by 3-body physics and molecular ion formation.

4.2 Theory of muonic hydrogen

Muonic hydrogen, an atom consisting of the proton and the muon is very similar to regular “electronic” hydrogen, so the theoretical description of the two atoms has many elements in common. The main difference is in the mass of the lepton. The muon is about 207 times heavier than the electron, and the muon-proton mass ratio η , according to NIST [3], is given by $\eta = 0.1126095272(28)$. This is not very small as is the case for $e\text{H}$, and therefore the static nucleus approximation is not necessarily the best starting point for the theoretical description of μH . Nevertheless, the traditional nonperturbative approach introduced by Borie and Rinker in a seminal work [74], continued by Borie [75, 76], and very recently by Indelicato [77] and Carroll *et al.* [78] is based on the Dirac equation and corrected for the finite nuclear mass by including some additional contributions. Here, we present an approach, symmetric in the proton and the muon, that can also be applied to electronic hydrogen. There are no significant numerical differences between both approaches [79], but the one presented below, to our opinion, is simpler and more elegant, since all the corrections can be accounted for in a

systematic way.

The binding energy E of a two-body system, according to quantum electrodynamics (QED) is a function of the fine structure constant α and of the muon-proton mass ratio $\eta = m_\mu/m_p$:

$$E = m_\mu \mathcal{E}(\alpha, \eta), \quad (6)$$

where we assume that both constituent particles are point-like. This binding-energy formula also neglects the presence of electron-positron pairs, which are incorporated through the Uehling potential discussed below. Even with these simplifications, there is no single equation which gives the exact binding energy, as is the case for the Dirac or Schrödinger equation. To some extent, the Bethe-Salpeter equation can be regarded as the most general bound state equation, but the kernel of this integro-differential equation can be given only perturbatively in the fine structure constant, and thus the exact solution is not known. In the approach presented here, traditionally called nonrelativistic quantum electrodynamics (NRQED), one expands the binding energy $\mathcal{E}(\alpha, \eta)$ in powers of the fine structure constant α , with $\alpha^{-1} = 137.035999074(44)$ and derives an exact closed formula for the expansion coefficients. In most cases these coefficients are expectation values of some effective Hamiltonian, and thus can easily be calculated.

The description of the QED bound two-body system begins with the leading order part, which is the nonrelativistic energy of two particles interacting via the Coulomb force in the reference frame with vanishing total momentum:

$$H_0 = \frac{p^2}{2m_\mu} + \frac{p^2}{2m_p} - \frac{\alpha}{r}. \quad (7)$$

According to the Schrödinger equation the binding energy is a function of the

principal quantum number only

$$E_0(n) = -\frac{m_r \alpha^2}{2n^2}, \quad (8)$$

where m_r stands for the reduced mass, and $\hbar = c = 1$. If so, the difference $\Delta E \equiv E_{LS}$ in binding energies of $2S_{1/2}$ and $2P_{1/2}$ states

$$E_{LS} \equiv E_{2P_{1/2}} - E_{2S_{1/2}} = 0. \quad (9)$$

Departures of E_{LS} from zero, traditionally called the Lamb shift, therefore arise from additional corrections to the energy.

The first set of corrections we discuss involves relativistic effects, although these are not the largest ones. In the static nucleus approximation the binding energy of $2S_{1/2}$ and $2P_{1/2}$ states according to the Dirac are also exactly the same. Moreover, the leading recoil corrections also do cancel, therefore relativistic effects in muonic hydrogen $\sim \eta^2 \alpha^4$ and thus are quite small. How are these relativistic corrections calculated? According to the NRQED approach, the leading relativistic corrections can be expressed in terms of the so called Breit-Pauli Hamiltonian [80]

$$\begin{aligned} H_{BP} &= H_0 + \delta H_{BP} \\ \delta H_{BP} &= -\frac{p^4}{8m_\mu^3} - \frac{p^4}{8m_p^3} - \frac{\alpha}{2m_\mu m_p} p^i \left(\frac{\delta^{ij}}{r} + \frac{r^i r^j}{r^3} \right) p^j \\ &\quad + \frac{2\pi\alpha}{3} \left(\langle r_p^2 \rangle + \frac{3}{4m_\mu^2} + \frac{3}{4m_p^2} \right) \delta^3(r) \\ &\quad + \frac{2\pi\alpha}{3m_\mu m_p} g_\mu g_p \vec{s}_\mu \cdot \vec{s}_p \delta^3(r) - \frac{\alpha}{4m_\mu m_p} g_\mu g_p \frac{s_\mu^i s_p^j}{r^3} \left(\delta^{ij} - 3 \frac{r^i r^j}{r^2} \right) \\ &\quad + \frac{\alpha}{2r^3} \vec{r} \times \vec{p} \left[\vec{s}_\mu \left(\frac{g_\mu}{m_\mu m_p} + \frac{(g_\mu - 1)}{m_\mu^2} \right) + \vec{s}_p \left(\frac{g_p}{m_\mu m_p} + \frac{(g_p - 1)}{m_p^2} \right) \right], \end{aligned} \quad (10)$$

where \vec{s}_μ , \vec{s}_p are spin operators of the muon and the proton, and g_μ , $g_p = 5.585694712(46)$ are g -factors. The interaction δH_{BP} includes also the effect due to the finite proton charge radius r_p together with the Darwin terms in order to make it clear that these two effects are separated. H_{BP} was derived years ago

before NRQED was formulated, nevertheless we use it as a part of the NRQED approach. The related correction to energy, neglecting terms with the proton spin \vec{s}_p , the proton charge radius r_p and assuming $g_\mu = 2$, (corrections due to $g_\mu - 2$ are included later as the muon self-energy)

$$\begin{aligned}\delta_{\text{rel}}E_{LS} &= \langle 2P_{1/2} | \delta H_{BP} | 2P_{1/2} \rangle - \langle 2S_{1/2} | \delta H_{BP} | 2S_{1/2} \rangle \\ &= \frac{\alpha^4 m_r^3}{48 m_p^2} = 0.05747 \text{ meV}\end{aligned}\quad (11)$$

is quite small, as expected. This means that the perturbative treatment of relativistic effects is very appropriate and higher order terms will be even smaller, if not negligible. In deriving (11), we neglected the hyperfine interaction. Although we are not interested here in the hyperfine splitting, this interaction leads to the mixing of $P_{1/2}$ and $P_{3/2}$ states and shifts these levels. This additional mixing correction was first considered in [81] and amounts to

$$\delta E_{LS}(P_{1/2}^{F=1}) = -0.1446 \text{ meV}, \quad (12)$$

and $E_{LS}(P_{3/2}^{F=1}) = +0.1446 \text{ meV}$. By definition, we do not include this as part of the Lamb shift, but consider it as a separate shift of $P_J^{F=1}$ levels, see Fig. 4.

So far we showed that the α^2 relativistic effects are relatively small. Indeed, the leading effect on the Lamb shift comes from vacuum polarization effects. Namely, the Coulomb interaction between the muon (electron) and the proton is modified by creation of the electron-positron pairs in the electric field. In the language of quantum electrodynamics the photon propagator includes closed fermion loop corrections, what results in the modification of the Coulomb interaction by the so called Uehling potential

$$V_{\text{vp}}(r) = -\frac{Z\alpha}{r} \frac{\alpha}{\pi} \int_4^\infty \frac{d(q^2)}{q^2} e^{-m_e q r} u(q^2). \quad (13)$$

where

$$u(q^2) = \frac{1}{3} \sqrt{1 - \frac{4}{q^2}} \left(1 + \frac{2}{q^2} \right). \quad (14)$$

The characteristic range of the electron vacuum polarization $V_{\text{vp}}(r)$ is about the electron Compton wavelength, which is close to the Bohr radius in μH . Namely the ratio $\beta = m_e/(m_r \alpha) = 0.737386$ is not far from one. This means that the parameter β must be kept intact in making expansions in α , because the muon nonrelativistic wave function has a significant overlap with the electronic vacuum polarization potential V_{vp} . As a result, the vacuum polarization correction is large for muonic hydrogen, in contrast to that in the electronic hydrogen. Indeed, the leading vacuum polarization correction

$$\delta_{\text{vp}} E_{LS} = \langle 2P_{1/2} | V_{\text{vp}} | 2P_{1/2} \rangle - \langle 2S_{1/2} | V_{\text{vp}} | 2S_{1/2} \rangle = 205.0073 \text{ meV} \quad (15)$$

is the dominating part of the muonic hydrogen Lamb shift [81], and all other corrections are at least two orders of magnitude smaller. Note, that the expectation value is taken with nonrelativistic wave function and the muon-proton mass ratio η is included exactly. At first glance this procedure is less accurate than the expectation value taken with Dirac wave function, but we point out that the use of the reduced mass in the Dirac equation is more than questionable, because the leading relativistic recoil correction is not properly accounted for by using the reduced mass. In the present discussion, the vacuum polarization effects are treated perturbatively by taking expectation values instead of solving numerically the Schrödinger equation with this potential. Higher-order effects obtained by solving the Dirac equation can be included in the perturbative approach by including the higher-order terms as well. The slight advantage of perturbative approach is that the vacuum polarization potential acquires higher order QED corrections (two- and three-loops), therefore it is also known pertur-

batively, so higher order perturbation and loop corrections are treated on equal footing. Namely the second order correction due to the Uehling potential,

$$\delta E_{LS} = 0.1509 \text{ meV}, \quad (16)$$

is combined with the two-loop vacuum polarization (one-particle reducible and irreducible two-loop diagrams)

$$\delta E_{LS} = 1.5081 \text{ meV}. \quad (17)$$

The last correction is clearly the dominant one. Although much smaller, the complete α^3 correction due to electronic vacuum polarizations is included also in present μH theory. It was calculated, first by Kinoshita in [82], and later slightly corrected by Karshenboim *et al.* in Ref. [83]. The final result is

$$\delta E_{LS} = 0.0053 \text{ meV}. \quad (18)$$

The higher order (4-loops or more) vacuum polarization corrections are negligible at present. There are however additional vacuum polarization corrections, which are quite interesting. The electron-positron pairs are distorted by the presence of the real particles. Namely, these pairs can additionally interact with the muon or with the proton. This leads to three box type of diagrams, and the overall effect as obtained by Karshenboim *et al* [84]

$$\delta E_{LS} = -0.00089(2) \text{ meV}, \quad (19)$$

is almost negligible, as these three diagrams tend to cancel out. We nevertheless include them in the overall theoretical predictions to demonstrate that vacuum-polarization effects are calculated as completely as possible, and no significant effects are being neglected.

There are also vacuum polarization correction from muon pairs, and this effect is included later together with the muon self-energy. Finally the hadronic vacuum polarization, considered in detail in the context of the muon $g-2$, amounts to [85]

$$\delta_{\text{hvp}}E_{LS} = 0.0112(4) \text{ meV}. \quad (20)$$

Up to this point, all the vacuum polarization corrections has been calculated using the nonrelativistic wave function. The relativistic $O(\alpha^2)$ effects combined with evp (electron vacuum polarization) are included separately as another correction. Again, the muon-proton mass ratio η is treated exactly, so the use of Dirac equation is not appropriate. Instead, we introduce vacuum polarization effects in the Breit-Pauli Hamiltonian. This is achieved as follows. One notes from Eq. (13) that the evp corrected Coulomb interaction can be represented as a Coulomb interaction obtained with the exchange of massive photons, integrated with the mass dependent weight function. So, one derives the modified Breit-Pauli Hamiltonian $\delta_{\text{vp}}H_{BP}$ obtained using the massive photon, neglects the hyperfine interaction and finds that the corresponding correction to binding energy is

$$\delta_{\text{vp,rel}}E_{LS} = \langle \delta_{\text{vp}}H_{BP} \rangle + 2 \langle V_{\text{vp}} \frac{1}{(E - H)'} H_{BP} \rangle. \quad (21)$$

The resulting contribution to the Lamb shift was first calculated in [81], however with some errors. The correct result was first obtained by Jentschura in [86] and confirmed by Karshenboim in [87] and amounts to

$$\delta_{\text{vp,rel}}E_{LS} = 0.01876 \text{ meV}. \quad (22)$$

If one used the Dirac equation in the infinite nuclear mass limit, the obtained result 0.021 meV would differ significantly from (22). Nevertheless, this correction is quite small, as any relativistic correction for μH , so higher order relativistic

effects combined with evp can safely be neglected.

What next? In electronic hydrogen the dominating part of the Lamb shift is the electron self-energy. In the case of μH it is a small but nevertheless important correction. The formula for the one-loop Lamb shift in $e\text{H}$ is well known [7], the resulting correction in μH is obtained by replacement of the electron mass by the muon mass with the result

$$\delta E = -0.6677 \text{ meV}. \quad (23)$$

Further related corrections arise from including both muon self-energy and electron vacuum polarization effects. The calculation is not very simple as it involves modifying Bethe logarithms by evp. The complete calculation was performed by Jentschura [88] and the resulting correction is

$$\delta E = -0.0025 \text{ meV}. \quad (24)$$

We pass now, to remaining corrections which have an overlap with the proton elastic structure and polarizability effects, and not always are treated consistently in the literature. The pure recoil corrections of order α^5 , derived originally by Salpeter, assume that both particles have spin 1/2 and are point-like. They can not be obtained from the Dirac equation by including the reduced mass, as the Dirac energy is even in α . Their derivation requires a full QED treatment and the obtained result [7]

$$E(n, l) = \frac{m_r^3}{m_\mu m_p} \frac{(Z\alpha)^5}{\pi n^3} \left\{ \frac{2}{3} \delta_{l0} \ln \left(\frac{1}{Z\alpha} \right) - \frac{8}{3} \ln k_0(n, l) - \frac{1}{9} \delta_{l0} - \frac{7}{3} a_n - \frac{2}{m_p^2 - m_\mu^2} \delta_{l0} \left[m_p^2 \ln \left(\frac{m_\mu}{m_r} \right) - m_\mu^2 \ln \left(\frac{m_p}{m_r} \right) \right] \right\}, \quad (25)$$

where

$$a_n = -2 \left(\ln \left(\frac{2}{n} \right) + \left(1 + \frac{1}{2} + \dots + \frac{1}{n} \right) + 1 - \frac{1}{2n} \right) \delta_{l0} + \frac{1 - \delta_{l0}}{l(l+1)(2l+1)}, \quad (26)$$

is valid for an arbitrary mass of orbiting particles. Later, in the next section, we consider the elastic and inelastic two-photon exchange contribution, and this Salpeter correction has to be consistently subtracted out from the elastic amplitude. Coming back to pure recoil effects in μH , the resulting correction is

$$\delta E_{LS} = -0.0450 \text{ meV}. \quad (27)$$

The last correction we consider is due to the proton self-energy and the related definition of the proton charge radius [81]. We mention in passing that for an arbitrary spin I nucleus the charge radius is defined in NRQED by the effective coupling

$$\delta H = -e \left(\frac{\langle r_p^2 \rangle}{6} + \frac{\delta_I}{M^2} \right) \vec{\nabla} \cdot \vec{E}, \quad (28)$$

where \vec{E} is the electric field external to the proton. For a spinless nucleus $\delta_0 = 0$, for half-spin $\delta_{1/2} = 1/8$, what corresponds to the so called Darwin-Foldy term. We point out for future considerations that for higher spins there is no unique value of δ_I . Here, the muon is point-like, so its charge radius by definition vanishes, and the charge radius of the proton, the main issue of this review, is defined by the above equation. This definition would be equivalent to that obtained from the slope of $G_E(Q^2)$ form factor at $Q^2 = 0$, if the electromagnetic form factors are meaningful at an arbitrarily high precision level. This is not necessarily the case because of QED radiative corrections. The proton self energy leads to the modification of elastic form factors in such a way that they depend on a fictitious photon mass, or in other words, are no longer well defined. The only correct definition has to employ complete two-photon structure functions, but this will not be analyzed here. We take the simplest possible point of view and use the

formula for the low energy part of the proton self-energy

$$E(n, l) = \frac{4 m_r^3 (Z^2 \alpha) (Z \alpha)^4}{3 \pi n^3 m_p^2} \left(\delta_{l0} \ln \left(\frac{m_p}{m_r (Z \alpha)^2} \right) - \ln k_0(n, l) \right). \quad (29)$$

The corresponding correction in μH is

$$\delta E_{LS} = -0.0099 \text{ meV}. \quad (30)$$

The high energy part of the Lamb shift is by definition included in the proton formfactors, more precisely in the charge radius and the magnetic moment anomaly. The problem which remains is how this definition corresponds to the proton charge radius as obtained from the electron scattering. We do not aim to analyze it, because possible inconsistencies are much smaller than the observed discrepancy between μH and the electron scattering determination of r_p .

All corrections presented in this section sum to

$$\Delta E_{LS} = 206.0330 \text{ meV}. \quad (31)$$

There are many further small QED corrections considered in the literature which are higher order in α or in powers of vacuum polarization. The main purpose of these further calculations was to find a possible missing large correction. However, no significant QED correction has been found yet, which would explain the discrepancy, but in principle we can not exclude its existence.

All known corrections have been summarized recently by Antognini *et al.* [79], and we refer readers to that work for more details. Their value (Eq.(32) below) differs only slightly from that in Eq. (31).

The calculation of the fine and hyperfine splittings [89], see Fig. 4, except for $E_{\text{HFS}}^{2S_{1/2}}$ is much simpler, so we present here only the final numerical results [79]

$$\Delta E_{\text{LS}} = 206.0336(15) - 5.2275(10) r_p^2 + \Delta E_{\text{TPE}}$$

$$\begin{aligned}
\Delta E_{\text{FS}} &= 8.3521 \text{ meV} \\
\Delta E_{\text{HFS}}^{2S_{1/2}} &= 22.8089(51) \text{ meV, (exp. value)} \\
\Delta E_{\text{HFS}}^{2P_{1/2}} &= 7.9644 \text{ meV} \\
\Delta E_{\text{HFS}}^{2P_{3/2}} &= 3.3926 \text{ meV} \\
\Delta &= 0.1446 \text{ meV}
\end{aligned} \tag{32}$$

where $\Delta E_{\text{TPE}} = 0.0351(20) \text{ meV}$ (see Table 1) is a proton structure dependent two-photon exchange contribution, which is considered in the next section. The theoretical value for $2S_{1/2}$ hyperfine splitting is uncertain due to not well known proton-structure effects in magnetic interactions, so the above value is the experimental one, taken from [2].

4.3 Proton Polarizability Effect in Muonic Hydrogen

The previous subsection is concerned with the QED calculations needed to determine the proton radius from the muonic energy level splittings between $2P$ and $2S$ states. There is one particular term, occurring at the intersection between QED and strong interaction effects which is deserving of special attention. This is the proton polarizability contribution that enters in the two-photon exchange term, see Fig. 5. The computed effect of this term is proportional to the lepton mass to the fourth power, and so is capable of being relevant for muonic atoms, but irrelevant for electronic atoms.

The proton can be excited by the absorption of a photon and then de-excited by the emission of a photon. Thus the two-photon exchange term depends on the forward virtual photon-proton (Compton) scattering amplitude $T^{\mu\nu}(\nu, q^2)$ where q^2 is the square of the four momentum, q^μ of the virtual photon and ν is its time

component. The contribution of the graph of Fig. 5 is given by the expression [90]:

$$E = -\frac{e^4}{2}\phi(0)^2 \int \frac{d^4q}{(2\pi)^4} \frac{1}{q^4} [T^{\mu\nu} - t^{\mu\nu}(M)] t_{\mu\nu}(m), \quad (33)$$

where $t^{\mu\nu}$ is the Compton amplitude for a pointlike fermion of mass M (proton) or m (muon), $\phi^2(0) = \frac{\alpha^3 m_r^3}{8\pi}$ for the 2S state with m_r as the lepton reduced mass. The role of the term $t^{\mu\nu}(M)$ in Eq. (33) is to subtract the term recoil correction discussed in the previous section. Using Eq. (33) still requires the subtraction of the infrared divergent term related to the QED correction to the proton charge radius discussed in the previous section.

The quantity $T^{\mu\nu}(\nu, q^2)$ is decomposed into a combination of two independent terms, $T_{1,2}(\nu, q^2)$, allowed by symmetries. The imaginary parts of the functions $T_{1,2}(\nu, q^2)$ are related to structure functions $F_{1,2}$ measured in electron- or muon-proton scattering, so that $T_{1,2}$ can be expressed in terms of $F_{1,2}$ through dispersion relations. However, $F_1(\nu, Q^2)$ falls off too slowly for large values of ν for the dispersion relation to converge. Hence, one makes a subtraction at $\nu = 0$, requiring that a new function of Q^2 , $\bar{T}_1(0, Q^2)$, be introduced. The contributions to the Lamb shift are broken into three terms [91]: $E = \Delta E^{el} + \Delta E^{inel} + \Delta E^{subt}$, where *el* refers to lepton-proton intermediate states, *inel* refers to intermediate excitations of the proton, and *subt* refers to the subtraction term. This separation into three terms is somewhat arbitrary, as emphasized by Ref. [92]. But so far no authors have found that differences between different possible separations are relevant for resolving the proton radius puzzle.

The subtraction term has typically been handled by using a power series expansion around $Q^2 = 0$, and then using effective field theory to determine the

coefficients of the series. In practice, people [90, 91, 93, 94] have used

$$\bar{T}_1(0, Q^2) = \frac{\beta_M}{\alpha} Q^2 F_{\text{loop}}(Q^2), \quad (34)$$

where $F_{\text{loop}}(Q^2)$ is a function that falls with Q^2 sufficiently rapidly so that the necessary integral converges. The calculations of three groups are summarized in Table 1. The theoretical uncertainty as determined from the three values of ΔE shown in the Table would seem to be very small. However, there is a hint of trouble in the large relative differences between the values for ΔE^{subt} . Birse & McGovern [94] reevaluated the subtraction term (using the separation of terms employed by Ref. [91]) and computing one order higher in the power series for Q^2 , to find $\Delta E^{\text{subt}} = 4.2 \pm 1.0 \mu\text{eV}$. Some authors [92, 95–97] have argued that the uncertainty in this term is substantial, even though the typical values are only a few μeV , very small compared to the 310 μeV needed to account for the proton radius puzzle.

The trouble is that the integral that determines ΔE^{subt} [97] would diverge logarithmically without the introduction of the form factor $F_{\text{loop}}(Q^2)$. In principle, one needs to evaluate an infinite set of terms in the power series describing $\bar{T}_1(0, Q^2)$ and hope that the result would lead to a convergent integral. Miller [97] used the form

$$F_{\text{loop}}(Q^2) = \frac{Q^4}{M_\gamma^4} \frac{1}{(1 + aQ^2)^3}. \quad (35)$$

The use of this form allows one to state the expression for the energy shift in closed form, which is well approximated by

$$\Delta E^{\text{subt}} \approx \frac{3}{2} m \alpha \phi^2(0) \frac{\beta_M}{M_\gamma^4 a^2}. \quad (36)$$

Using, $M_\gamma = 0.5 \text{ GeV}$ and $a = 0.0078/(4m_\mu^2) = 0.177 \text{ GeV}^{-2}$ led to value of the Lamb shift of 0.31 meV. A relatively large value of $1/a$ must appear to obtain

the necessary contribution, but no fundamental principles have been violated.

Thus the above discussion shows that procedures used to estimate the size of the subtraction term suffer from significant uncertainties. This arises because the chiral EFT is being applied to the virtual-photon nucleon scattering amplitude, and as a result the energy shift depends on an integral that would be logarithmically divergent if the function F_{loop} were replaced by unity. Another way to proceed would be us to use an effective field theory (EFT) for the lepton-proton interaction.

In EFT logarithmic divergences identified through dimensional regularization are renormalized away by including a lepton-proton contact interaction in the Lagrangian. This was done [97] by using standard dimensional regularization (DR) techniques by evaluating the scattering amplitude of Fig. 5. The term of interest is obtained by including only $\bar{T}_1(0, Q^2)$ of Eq. (34) with $F_{\text{loop}} = 1$. The result is :

$$\mathcal{M}_2^{DR}(\text{loop}) = \frac{3}{2}i \alpha^2 m \frac{\beta_M}{\alpha} \left[\frac{2}{\epsilon} + \log \frac{\mu^2}{m^2} + \frac{5}{6} - \gamma_E + \log 4\pi \right] \bar{u}_f u_i \bar{U}_f U_i, \quad (37)$$

where lower case spinors represent leptons of mass m , and upper case proton of mass M , γ_E is Euler's constant, $0.577216 \dots$, μ is the parameter introduced in using dimensional regularization and one works in a space of dimension $d = 4 - \epsilon$.

The result Eq. (37) corresponds to an infinite contribution to the Lamb shift in the limit that ϵ goes to zero. In EFT one removes the divergent piece by adding a lepton-proton contact interaction to the Lagrangian that removes the divergence, replacing it by an unknown finite part. The finite part is obtained by fitting to a relevant piece of data. Here the only relevant data is the 0.31 meV needed to

account for the proton radius puzzle. When this is done the result is

$$\mathcal{M}_2^{DR} = i \, 3.95 \, \alpha^2 m \frac{4\pi}{\Lambda_\chi^3} \bar{u}_f u_i \bar{U}_f U_i. \quad (38)$$

where the results are expressed in terms of the chiral symmetry breaking scale $\Lambda_\chi \equiv 4\pi f_\pi$, (f_π is the pion decay constant). The coefficient 3.95 is of natural size. Thus standard EFT techniques result in an effective lepton-proton interaction of natural size that is proportional to the lepton mass.

The present results, Eq. (36) and Eq. (38) represent an assumption that there is a lepton-proton interaction of standard-model origin, caused by the high-momentum behavior of the virtual scattering amplitude, that is sufficiently large to account for the proton radius puzzle. This assumption needs further testing. Fortunately, our hypothesis can be tested in an upcoming low-energy $\mu^\pm p, e^\pm p$ scattering experiment that is discussed in Sect. 5.2.

4.4 Theory of hydrogen energy levels

One of the possible explanations for the proton charge radius puzzle is that it is caused by a mistake or a missing correction in the hydrogen Lamb shift theory. We will argue that this is the least probable solution. Why? It is because corrections to the hydrogen Lamb shift have been calculated by many groups using different methods, with only few exceptions which are described below in detail. For a recent review of Hydrogen theory in the context of determination of the proton charge radius see Ref. [3].

All the corrections to the Lamb shift are classified in powers of α , $Z\alpha$ and the mass ratio m_e/m_p , where the power of α counts the number of loops. The additional proton structure corrections, elastic and inelastic two-photon contributions are of the order of tens of Hz for 1S state [3], while the discrepancy in

the proton charge radius corresponds to about 100 kHz. So, any proton structure effect beyond the the finite size correction is negligible.

The leading contributions to the hydrogen Lamb shift, the one-loop electron self-energy and the vacuum polarization have been calculated by an expansion in $Z\alpha$ [98] or directly numerically [99], using the known form of the relativistic electron propagator in the Coulomb field. Both methods are in agreement, but the numerical one is presently more accurate, about a few Hz for the ground state, so there is no room for any mistake of order of 100 kHz.

The two-loop contribution has also been calculated numerically [100] and analytically [98,101], but the results differ slightly. Numerical calculations have been performed only for the nuclear charge $Z \geq 10$ and the result for $Z = 1$ was obtained by extrapolation. The analytic calculation was numerically accurate, but some higher order terms were omitted, because they are too difficult to evaluate. The final result is taken as an arithmetic mean with an uncertainty that matches both values. This uncertainty corresponds to about 2 kHz for 1S state, much too small to explain the discrepancy.

The three loop contribution in the leading order of $Z\alpha$ has been calculated only by one group [102]. This correction can be represented in terms of three-loop electromagnetic form factors of the free electron. Although technically very advanced, the conceptually simple methods of the evaluation of Feynman diagrams can be applied, so we do not expect a mistake here. The binding corrections, next order in $Z\alpha$ are known only partially [103], but can be roughly estimated to be about ~ 1 kHz.

The pure recoil effects, two-body diagrams without self-energy and vacuum polarization, although small, are not very simple to evaluate because the full

QED formalism must be used. The derivation of the closed formula for the pure recoil correction was achieved independently by two groups [104, 105]. The numerical evaluation was performed by analytic expansion in $Z\alpha$ [105, 106] and directly numerically [107]. Both are in agreement.

The radiative recoil corrections have been calculated only by $Z\alpha$ expansion, but independently by two groups [108, 109]. The overall result is rather small, some logarithmic higher order terms are also known [3], and remaining higher corrections are irrelevant at the order of discrepancy.

In conclusion there is no room for any new correction, or any mistake in the present calculations that would shift 1S Lamb shift by about 100 kHz.

4.5 Physics Beyond the Standard Model

The possibility that the proton radius puzzle might be caused by a difference between the μp and $e p$ interactions is very exciting because such an effect is not part of the Standard Model (SM). Awareness of the possibility of such a failure of what is known as electron-muon (or more generally lepton) universality was re-awakened by the muon $g-2$ experiment [110–112]. The experimental value of the muon anomalous magnetic moment a_μ exceeds the SM expectation by more than three standard deviations: $\Delta a_\mu \equiv a_\mu^{\text{exp}} - a_\mu^{\text{th}} = (29 \pm 9) \times 10^{-10}$. This difference could be caused by a new interaction. In addition, new gauge forces mediated by particles in the MeV-GeV scale could be dark matter candidates [113–115]. Obtaining a theory or model that could account for the proton radius puzzle, the muon anomalous magnetic moment and predict other new verified phenomena would be a tremendous breakthrough. However, it is not easy to invent new interactions that differentiate between electrons and muons because the principle

of lepton universality is very well tested.

The most relevant constraints of lepton universality have been nicely summarized in Refs. [116, 117]. The basic ideas are to use the non-observation of new particles that couple only to muons and to search for differences between muonic and electronic decays of various particles. Constraints are obtained from the decay of the Υ resonances [118–120]; neutron interactions with nuclei [121–123]; the anomalous magnetic moment of the muon [112]; x-ray transitions in ^{24}Mg and ^{28}Si atoms; J/Ψ decay [124]; neutral pion decay [125]; and eta decay [126].

Barger *et al.* [116] postulate the existence of new interactions mediated by the exchange of a boson between muons and nucleons. To explain the proton radius puzzle, these exchanges must give rise to an attractive interaction that accounts for 0.31 meV. One can include the exchange of scalar, vector and tensor bosons. Axial vector exchange gives a spin-spin interaction that affects the hyperfine splitting, but not the Lamb shift, and is not considered further in Ref. [116].

Given the non-relativistic motion of the muon and the nucleon, the exchange of boson between the muon and nucleon leads to a Yukawa interaction :

$$\Delta V(r) = -\alpha_\chi \frac{e^{-m_\chi r}}{r}, \quad (39)$$

where m_χ is the mass of the postulated boson and α_χ is the product of lepton- and nucleon-boson coupling constants divided by 4π . Assuming sufficiently weak couplings, first order perturbation theory can be used to obtain the contribution to the muon Lamb shift [74] as

$$\delta(\Delta E) = \alpha_\chi m_\chi \frac{\frac{m_\chi}{\alpha m_r}}{2(1 + \frac{m_\chi}{\alpha m_r})^2}, \quad (40)$$

where the muon-nucleon reduced mass is m_r .

Barger *et al.* conclude that new spin 0,1 and 2 particles that mediate flavor-

conserving non universal spin-independent interactions are excluded. This finding depends on assuming that the new particles couple only to the muon, and that the coupling to mesons is the same as to the nucleon.

Brax & Burrage [127] note that light scalar mesons coupled to matter appear in many fundamental contexts, such as in the inflationary scalar field and in attempts to unify gravity with the standard model. However, these interactions are strongly constrained by experimental searches for fifth forces, and violations of the equivalence principle. Non-linear dynamics [128–130] can be introduced to avoid these constraints. Brax & Burrage use the assumption that matter couples universally to the scalar field to obtain a new stringent bound on the coupling of scalar fields to matter from the precise measurements of the difference between the energies of the 1s and 2s states in hydrogen, while the coupling to photons is constrained by the Lamb shift. The net result of these considerations is that the contribution of a scalar field to the discrepancy between proton radii measured in electronic and muonic atoms is negligible.

Tucker-Smith & Yavin [131] go through a chain of reasoning similar to that of Barger *et al.* [116], and find that a new force carrier with mass of order MeV that couples to protons and muons can account for the proton radius puzzle as well as the difference between QED and measurements for $g - 2$ of the muon. They acknowledge that many constraints exist, but state that none of the existing constraints exclude such a force in a model-independent manner. The difference in conclusion with Barger *et al.* arises because Tucker-Smith & Yavin do not assume universal couplings to nucleons and mesons. Tucker-Smith & Yavin state that their postulated force can be tested in measurements of muonic-deuterium and helium.

Motivated by the interest in the possibility of new gauge forces the mediate interactions between dark matter and standard model parameters, Batell *et al.* [132] use a model in which a new $U(1)$ gauge boson (heavy photon) is kinetically mixed with hypercharge. New scalar and vector force carriers interact with right-handed neutrinos. Current experiments at JLab, Mainz, KLOE and BaBar are searching for such particles but haven't found any. This limits the value of the mass of the heavy photon to be about 30 MeV. If the strength of this particular new force is large enough to account for the proton radius puzzle, parity violating asymmetries in muon-nucleon or muon-nucleus scattering would be enhanced by several orders of magnitude and would be of order 10^{-4} . Ref. [117] use the nonobservation of missing mass events in the lepton kaon decay $K \rightarrow \mu\chi$ to find strong constraints on parity-violating gauge interactions of a right handed muon provided χ decays invisibly or does not decay inside the detector.

Carlson & Rislow [133] consider two models, one containing scalar and pseudo scalar particles and the other vector and axial vector particles. The basic idea is that the scalar or vector particles account for the Lamb shift while the pseudoscalar and axial vector particles do not contribute. Large effects in the muon $g - 2$ are prevented by cancellations between the effects of scalar (vector) and pseudoscalar (axial) mesons. Constraints on the masses of the new particles are obtained from the nonobservation of such particles in kaon decays. Exchanges of pseudoscalar and axial vector particles contribute to hyperfine splittings, and the resulting constraints are not considered in Ref. [133].

It is also worthwhile to discuss the possible influence of new forces on the PSI muon-proton scattering experiment (Sect. 5.2). If the new particles are light, they act like a very small modification of the Coulomb force and can not be

detected. If the new particles are sufficiently heavy, the force between the muon and the proton is well-approximated by a contact interaction (as in the model [97] discussed in Sect. 3e) and its effects are detectable as an interference between a short-ranged and long-ranged Coulomb interaction.

To summarize, there are many constraints on new forces. Some of these constraints are derived from model-dependent considerations, and the new force possibility remains viable for a subspace of all of the relevant parameters. The ultimate disposition of this possibility will depend on either directly detecting the postulated particles or directly verifying an independent prediction of one of these models.

5 New projects

There is an interesting set of new experiments that could shed light on the proton radius puzzle.

5.1 New electron scattering experiments

Improving the precision of the radius determination from electron scattering experiments requires that cross sections be measured with higher precision and/or to smaller Q^2 . All higher precision measurements that have been done to date have used magnetic spectrometers with small or moderate solid angle acceptance, and it is hard to see how a significant improvement can be made in the precision of these measurements. As $Q^2 \approx 4EE' \sin^2(\theta/2)$, going to smaller Q^2 requires smaller scattering angles and/or beam energies. But the magnetic spectrometers have limited angular ranges, and the experiments already run have used the lowest beam energies available at modern accelerators. Thus, an improved electron

scattering experiment requires a different technique.

The only experiment currently approved to improve the electron scattering radius determination is Jefferson Lab E12-11-106 [134], which aims to extend the Q^2 range of electron scattering experiments from the 0.0038 GeV² of the Mainz experiment down to about 10⁻⁴ GeV². The experiment has several novel features that combine to allow a significant radius determination from a measurement only at low Q^2 . Low current, 1 and 2 GeV beams in Hall B impinge upon an open-ended hydrogen gas cell, as has been used in storage rings previously, to eliminate the need to subtract target end cap backgrounds. The spectrometer, the PRIMEX HYCAL (PbWO₄) calorimeter, will cover the entire angle range of ≈ 10 mrad - 70 mrad in one setting, to cover the Q^2 range 10⁻⁴ GeV² \rightarrow 10⁻² GeV². Moller scattering of the beam from atomic electrons will provide the data used to determine the detector solid angles, offsets, and efficiencies at the high level needed. The lower energy of the Moller scattered electrons allows the two reactions to be distinguished by the calorimeter.

The difference in the cross sections arising from the difference in the measured radii is small, requiring high precision cross section measurements. Approximating $G_E = 1 - Q^2 r_p^2 / 6$, radii of 0.842 fm vs. 0.875 fm lead to differences in the cross sections of 0.005%, 0.05%, 0.5% and 1.0% for Q^2 of 10⁻⁴ GeV², 10⁻³ GeV², 0.01 GeV² and 0.02 GeV², respectively, and differences half that large for the form factor. Existing electron experiments each are about 5σ different from the muonic hydrogen result. If the radius is to be determined to give a similar quality result, then relative cross sections need to be determined at the 0.2% level. The large cross sections and event rates for low Q^2 scattering are large, making statistical uncertainties at the 0.1% quite feasible.

Systematic uncertainties must also be controlled at a level that would be very difficult without a well understood calibration reaction. Reaching low Q^2 requires small scattering angles and/or beam energies. With a 1 GeV beam energy, reaching 10^{-3} (10^{-4}) GeV^2 requires a scattering angle of 32 (10) mrad. But the Mott cross section diverges at small angles due to the $1/\sin^4(\theta/2)$ factor, leading to a shift in the cross section of $0.01\%/\mu\text{rad}$ ($0.03\%/\mu\text{rad}$) at 10^{-3} (10^{-4}) GeV^2 . A 10 μrad knowledge of the scattering angle is then needed to limit shifts the relative cross sections by 0.2%. In contrast, typical high precision electron scattering experiments with magnetic spectrometers determine absolute scattering angles at about the 1 mrad level.

Jefferson Lab E12-11-106 is approved and tentatively scheduled to run in 2014-2015. If various technical challenges are met, it has an excellent chance of resolving all experimental questions related to data normalizations and fits used to extract the proton radius from electron scattering experiments, either confirming the puzzle, or resolving it as being due to incorrect radius extractions from the electron (scattering) data.

5.2 Elastic muon-proton scattering

The missing measurement in determining the proton radius with muons and electrons is muon scattering, a measurement that the MUon proton Scattering Experiment (MUSE) collaboration proposes at PSI [135]. Muon scattering is not an easy measurement, as muons are produced as secondary beams from the decays of π 's produced from a primary proton beam. As a result, muon beams have low flux and large emittance, compared to electron beams. Unless efficient particle separators are available, the muon beam will also include background

pions and electrons.

The proposed MUSE experiment is based at the PSI π M1 beam line. The beam line provides of order MHz muon fluxes for momenta from about $100 \rightarrow 250$ MeV/ c . To handle the multiple particle species in the beam, MUSE uses Scintillating Fiber arrays to determine RF time and only operates at momenta where the muon RF time is about 4 or more ns different from electron and pion RF times. A custom FPGA system will allow the RF time to be determined in hardware so that the information is available to the trigger. To avoid issues arising from accidental coincidences, MUSE intends to limit the channel acceptance to keep the total beam flux at ≈ 5 MHz. The large emittance of the beam requires the use of GEM chambers to track individual beam particles into the target, so that the scattering angle is sufficiently well known. Test measurements have largely verified that the beam properties are sufficient for the experiment.

The low rates also require a large acceptance spectrometer. MUSE is planning a nonmagnetic spectrometer, consisting of wire chambers and fast scintillators for triggering and particle identification. The main reason for this is that experiments with large acceptance detectors and magnetic fields do not measure precise cross sections.

MUSE intends to measure with both μ^+ and μ^- beams, so that two-photon effects can be directly determined from the data. MUSE also intends to measure both muon and electron scattering at the same time, so that the experiment can compare them.

The collaboration has studied singles rates, background triggers, and systematic uncertainties to estimate how well the cross sections, form factors, and radii from the various measurements can be compared. A number of difficulties arise

that are not present in electron scattering experiments. The π induced backgrounds are efficiently removed at the trigger level through the measurements of beam RF time, which is only possible due to the low beam flux. The beam muons decay, which is mainly a problem as the decay electrons cannot be distinguished from the muon scattering at the trigger level, and are not as easily distinguished with a non-magnetic spectrometer. Although the muon decay fraction is small, it is much larger than the scattering fraction. The muon radiative tail is very small, but electrons have a large radiative tail which must be handled. The beam emittance is large, requiring measurement by detectors in the beam, which further increases the emittance. Many of the systematic uncertainties are similar to electron scattering experiments, but the low energy muon beam has reduced sensitivity to angle offsets, radiative corrections, and hadronic backgrounds compared to a GeV electron beam. Preliminary estimates are that the radius can be extracted from muon scattering about as well as in the Mainz experiment, in part because the experiment can reach $Q^2 \approx 0.002 \text{ GeV}^2$, about half the lower limit of the Mainz measurement.

The MUSE experiment requires significant new funding ($\approx 2 \text{ M\$}$) to be carried out. It might be able to run as soon as 2016.

5.3 Spectroscopy of electronic atoms and ions

As detailed in Sect. 2.1, the value of r_p can be determined from the 1S-2S transition in H [25] using precisely calculated QED theory only if a sufficiently precise value of the Rydberg constant R_∞ is supplied. At present, R_∞ originates from several measurements of transition frequencies in H and D.

In fact, the correlation coefficient between R_∞ and r_p is 0.984 in the 2010

CODATA adjustment [3]. Hence, any new determination of the Rydberg constant at a level of a few parts in 10^{12} would help to shed new light on the proton radius discrepancy between electronic and muonic hydrogen.

Several such projects are underway. Flowers *et al.* at the British NPL are measuring the 2S-6S/D 2-photon transitions in atomic H [136]. Beyer *et al.* at MPQ, Garching [137], aim at an improved value of R_∞ from 1-photon transitions in H, namely the 2S-4P and higher P-states. This project utilizes for the first time a cryogenic beam of H atoms from a nozzle at 6 K, optically excited to the 2S state using the 1S-2S laser system [25]. This can eliminate possible systematic effects like dc-Stark shifts from patch charges caused by the electron bombardment traditionally used to create H(2S) atoms and align the H atom beam onto the laser beams. The cold atom beam can help to reduce systematic effects caused by the large velocity of traditional “hot” beams, but the 1-photon transition is particularly sensitive to 1st order Doppler shifts. The 1S-3S transition in H has recently been measured by Nez *et al.* at LKB, Paris [138]. It is the second best measured transition frequency in H, but as can be seen in Fig. 2 it does not provide the most precise r_p value when compared with 1S-2S following Eq. (4). This is because both the 1S-2S and the 1S-3S transition depend on the large 1S Lamb shift L_{1S} , and the “lever arm” on R_∞ is hence reduced. Nevertheless, this measurement is very valuable because it serves as a cross-check for the 1S-2S transition in H [25] which has for a long time been measured by only the MPQ group. The Paris group is improving their 1S-3S setup, in particular the laser system, and aims at a significant improvement of their accuracy [138]. The 1S-3S transition in H is also being measured at MPQ, Garching, by Peters and coworkers [139]. To overcome difficulties in the generation of the 205 nm light required

to drive the 1S-3S transition in H they use two counter-propagating picosecond frequency combs.

Laser spectroscopy of He atoms and H-like He^+ ions are pursued by Udem and colleagues at MPQ [140] and by Eikema and colleagues [141] and Vassen and colleagues [142], both in Amsterdam. Ultimately, this will allow a Rydberg constant determination using He atoms or ions. A precise value of the He nuclear charge radius is available from electron scattering experiments [143]. Soon, the Lamb shift in muonic helium ions [144] will improve this accuracy further (see Sect. 5.4).

An alternative route towards a new determination of R_∞ is pursued by Tan and coworkers at NIST [145]. Here, H-like highly charged ions (e.g. Ne^{9+}) are created in circular large- ℓ -states at high principal quantum number n and stored in a Penning trap. In large- ℓ -states the effect of the finite nuclear size on the energy levels is negligible, and measuring these highly charged ions at high n states ensures that the transition frequencies can be determined using lasers in the optical region.

Hessels *et al.* [146] at York University, Toronto, aim at a new measurement of the “classical” 2S-2P Lamb shift in H. This radio-frequency transition was last measured in 1994 [147]. The new direct measurement of the Lamb shift will yield a value of r_p that does not require the knowledge of R_∞ , so it is an independent cross-check of the optical 2S- $n\ell$ transitions in H and D that determine R_∞ today (see Sect. 2.1).

5.4 Spectroscopy of exotic atoms

Spectroscopy of exotic atoms will also contribute to the solution of the proton radius puzzle. Precision laser spectroscopy of purely leptonic systems like positronium ($\text{Ps} \equiv e^+e^-$) [148, 149] or muonium ($\text{Mu} \equiv \mu^+e^-$) [150] can test bound-state QED free from finite nuclear size effects. Improved spectroscopy of the 1S-2S transitions and the ground state hyperfine splittings are on the way or being prepared. Ps and Mu test QED in the electronic and muonic sectors, respectively.

Laser spectroscopy of muonic deuterium atoms will soon shed new light on the radius puzzle [151]. A new charge radius of the deuteron can be compared with the one obtained from the isotope shift of the 1S-2S transition of electronic H and D [152]. The muonic deuterium measurement may also give new insights into the question of nuclear polarizability (see Sect. 4.3).

The PSI project R-10.01 is going to measure the Lamb shift in muonic helium ions $\mu^3\text{He}$ and $\mu^4\text{He}$ [144]. The measurement will give a tenfold improved value of the charge radii of the stable helium isotopes, compared to the value from electron scattering [143]. Together with the new measurements of transitions in electronic He atoms or ions [140–142] the muonic helium Lamb shift will provide a cross-check of the proton radius puzzle at $Z=2$.

A future possibility may be the measurement of transitions in muonic Li, Be and B ions [153]. Accurate charge radius differences of these nuclei are known from electronic isotope shift measurements [154–156].

6 Conclusions

The proton radius puzzle is real. A physical parameter should not depend on the method of extraction. Yet here we have two highly precise methods based on electronic and muonic hydrogen atoms that disagree significantly. The possible origins of the disagreement are the subject of much of this text. To summarize: the possibilities are

- The electronic hydrogen experiments are almost, but not quite, as accurate as stated (Sect. 2.2).
- The QED calculations are almost, but not quite, as accurate as stated (Sect. 4.2).
- The two photon exchange term that depends on proton polarizability has not been correctly evaluated (Sect. 4.3).
- The electron and muon really do have different interactions with the proton (Sect. 4.4), so that there is physics beyond the Standard Model.

None of these possibilities seem very likely, but all must be pursued.

There are some tasks for theorists. While the results of many of the QED calculations have been reconfirmed, it is still possible that something is missing in the theory. Current theories of beyond the standard model physics are very primitive and need technical improvements before being realized as a complete gauge theory without anomalies. Better treatments of the two-photon exchange term could be very useful.

Much additional work by experimentalists is necessary, and any future progress is contingent upon continuing a strong experimental effort in diverse directions. The electronic hydrogen experiments need to be redone using modern techniques

(Sect. 5.3). A new high energy-low momentum transfer electron scattering measurement could reach the accuracy of the spectroscopic determinations and provide an independent confirmation or repudiation of the radius obtained from electronic hydrogen spectroscopy, Sect. 5.1. The proposed muon-proton scattering experiment (Sect. 5.2) would rule on theories of the two-photon exchange interaction and also on theories beyond the standard model. Discovery of the new particles required by theories beyond the standard model would make such theories believable. Exotic atoms, in which muons are bound to nuclei, would also rule on all possible theories, Sect. 5.4. Future work on positronium would put QED to detailed tests.

The proton is the only stable baryon and all of Life depends on it. It is important to understand the proton. Its radius should be a simple quantity to determine and understand, but this is not the case. Recent experimental results have not been understood. But future work will either reveal the true value of this radius, a better understanding of its structure, or a very unexpected feature of its interactions.

7 Acknowledgements

The authors would like to thank the participants of the 2012 ECT* Workshop on the Proton Radius Puzzle in Trento, Italy, for stimulating and exciting discussions. R.P. acknowledges support from the European Research Council (ERC), StG 279765 and thanks the members of the CREMA collaboration. R.G. was supported by the US National Science Foundation grant PHY 09-69239. The work of G.A.M. is partially supported by USDOE Grant No. DE-FG02-97ER-41014. He would like to thank C.E. Carlson, J.D. Carroll, J. Rafelski and A.W. Thomas for

useful discussions. K.P. was supported by NCN grant 2012/04/A/ST2/00105.

LITERATURE CITED

1. Pohl R, Antognini A, Nez F, Amaro FD, Biraben F, et al., *Nature* 466:213 (2010).
2. Antognini A, Nez F, Schuhmann K, Amaro FD, Biraben F, et al., *Science* 339:417 (2013).
3. Mohr PJ, Taylor BN, Newell DB, *Rev. Mod. Phys.* 84:1527 (2012), [arXiv:1203.5425 (physics.atom-ph)].
4. A1 Collaboration, Bernauer JC, Aschenbach P, Ayerbe Gayoso C, Böhm R, Bosnar D, et al., *Phys. Rev. Lett.* 105:242001 (2010), 1007.5076.
5. Miller GA, *Phys. Rev. Lett.* 99:112001 (2007), 0705.2409.
6. Miller GA, *Ann.Rev.Nucl.Part.Sci.* 60:1 (2010), 1002.0355.
7. Eides MI, Grotch H, Shelyuto VA, *Theory of Light Hydrogenlike Atoms* (Springer Tracts in Modern Physics **222**, 2006).
8. Bawin M, Coon S, *Phys. Rev. C* 60:025207 (1999), nucl-th/9906014.
9. Karplus R, Klein A, Schwinger J, *Phys. Rev.* 86:288 (1952).
10. Lehmann P, Taylor R, Wilson R, *Phys. Rev.* 126:1183 (1962).
11. Hand LN, Miller DG, Wilson R, *Rev. Mod. Phys.* 35:335 (1963).
12. Murphy II JJ, Shin YM, Skopik DM, *Phys. Rev. C* 9:2125 (1974).
13. Murphy II JJ, Shin YM, Skopik DM, *Phys. Rev. C* 10:2111 (1974).
14. Simon GG, Schmitt C, Borowski F, Walther VH, *Nucl. Phys. A* 333:381 (1990).
15. Zhan X, Allada K, Armstrong DS, Arrington J, Bertozzi W, et al., *Phys. Lett. B* 705:59 (2011), 1102.0318.

16. Wong CW, *Int. J. Mod. Phys.* 3:821 (1994).
17. Mergell P, Meissner UG, Drechsel D, *Nucl. Phys. A* 596:367 (1996), hep-ph/9506375.
18. Rosenfelder R, *Phys. Lett. B* 479:381 (2000), nucl-th/9912031.
19. Sick I, *Phys. Lett. B* 576:62 (2003), nucl-ex/0310008.
20. Belushkin MA, Hammer HW, Meissner UG, *Phys. Rev. C* 75:035202 (2007).
21. Sick I, *Few-Body Syst.* 50:367 (2011).
22. Mohr PJ, Taylor BN, Newell DB, *Rev. Mod. Phys.* 80:633 (2008).
23. Blunden PG, Sick I, *Phys. Rev. C* 72:057601 (2005).
24. Lamb WE, Retherford RC, *Phys. Rev.* 72:241 (1947).
25. Parthey CG, Matveev A, Alnis J, Bernhard B, Beyer A, et al., *Phys. Rev. Lett.* 107:203001 (2011), [arXiv: 1107.3101 (atom-ph)].
26. de Beauvoir F, Nez B, Julien L, Cagnac B, Biraben F, Touahri D, et al., *Phys. Rev. Lett.* 78:440 (1997).
27. Schwob C, Jozefowski L, de Beauvoir B, Hilico L, Nez F, et al., *Phys. Rev. Lett.* 82:4960 (1999).
28. Perdrisat C, Punjabi V, Vanderhaeghen M, *Prog.Part.Nucl.Phys.* 59:694 (2007), hep-ph/0612014.
29. Arrington J, de Jager K, Perdrisat CF, *J.Phys.Conf.Ser.* 299:012002 (2011), 1102.2463.
30. Jefferson Lab Hall A, Jones MK, et al., *Phys. Rev. Lett.* 84:1398 (2000), nucl-ex/9910005.
31. Arrington J, Blunden P, Melnitchouk W, *Prog.Part.Nucl.Phys.* 66:782 (2011), 1105.0951.
32. Arrington J, (2012), 1210.2677.

33. Crawford CB, Sindile A, Akdogan T, Alarcon R, Bertozzi W, et al., Phys. Rev. Lett. 98:052301 (2007), nucl-ex/0609007.
34. Ron G, Glister J, Lee B, Allada K, Armstrong W, et al., Phys. Rev. Lett. 99:202002 (2007), 0706.0128.
35. Jefferson Lab Hall A Collaboration, Ron G, et al., Phys. Rev. C 84:055204 (2011), 1103.5784.
36. Ron G, Mod.Phys.Lett. A26:2605 (2011).
37. Arrington J, Phys. Rev. Lett. 107:119101 (2011), 1108.3058.
38. Bernauer J, Achenbach P, Ayerbe Gayoso C, Bohm R, Bosnar D, et al., Phys. Rev. Lett. 107:119102 (2011).
39. Lorenz I, Hammer HW, Meissner UG, Eur. Phys. J. A 48:151 (2012), 1205.6628.
40. Bernauer JC, 2010, PhD thesis, Johannes-Gutenberg-Universität Mainz, Germany, URL wwwa1.kph.uni-mainz.de/A1/publications/doctor/bernauer.pdf.
41. Belushkin M, Hammer HW, Meissner UG, Phys. Rev. C 75:035202 (2007), hep-ph/0608337.
42. Hill RJ, Paz G, Phys. Rev. D 82:113005 (2010), 1008.4619.
43. Sick I, Few Body Syst. 50:367 (2011).
44. Sick I, Prog.Part.Nucl.Phys. 67:473 (2012).
45. Kelly JJ, Phys. Rev. C 70:068202 (2004).
46. Di Giacomo A, Nucl. Phys. B 11:411 (1969).
47. Bethe HA, Phys. Rev. 72:339 (1947).
48. Placci A, Polacco E, Zavattini E, Ziock K, Phys. Lett. B 32:413 (1970).
49. Anderhub H, Hofer H, Kottmann F, Coultre PL, Makowiecki D, et al.,

- Phys. Lett. B 71:443 (1977).
50. Egan PO, Dhawan S, Hughes VW, Lu DC, Mariam FG, et al., Phys. Rev. A 23:1152 (1981).
 51. Anderhub H, von Arb HP, Böcklin J, Dittus F, Ferreira Marques R, et al., Phys. Lett. B 143:65 (1984).
 52. Böcklin J, Ph.D. thesis ETHZ Nr. 7161 (1982).
 53. Pohl R, Antognini A, Nez F, Amaro FD, Biraben F, et al., Can. J. Phys. 89:37 (2011).
 54. Kottmann F, Daniel H, Hartmann FJ, Hauser P, Maierl C, et al., Hyp. Interact. 119:3 (1999).
 55. Pohl R, Daniel H, Hartmann FJ, Hauser P, Liu YW, et al., Hyp. Interact. 138:35 (2001).
 56. Pohl R, Daniel H, Hartmann FJ, Hauser P, Kottmann F, et al., Phys. Rev. Lett. 97:193402 (2006).
 57. Taqqu D, Biraben F, Conde CAN, Hänsch TW, Hartmann FJ, et al., Hyp. Interact. 119:311 (1999).
 58. Pohl R, Biraben F, Conde CAN, Donche-Gay C, Hänsch TW, et al., Hyp. Interact. 127:161 (2000).
 59. Kottmann F, Biraben F, Conde CAN, Donche-Gay C, Hänsch TW, et al., AIP Conf. Proc. 564:13 (2001).
 60. Pohl R, Hyp. Interact. 193:115 (2009).
 61. Antognini A, Amaro FD, Biraben F, Cardoso JMR, Conde CAN, et al., Opt. Comm. 253:362 (2005).
 62. Antognini A, Schuhmann K, Amaro FD, Biraben F, Dax A, et al., IEEE J. Quant. Electr. 45:993 (2009).

- 63. Giesen A, Hgel H, Voss A, Wittig K, Brauch U, Opower H, Appl. Phys. B 58:365 (1994).
- 64. Rabinowitz P, Perry B, Levinos N, IEEE J. Quant. Electr. 22:797 (1986).
- 65. Pohl R, Antognini A, Amaro F, Biraben F, Cardoso J, et al., Can. J. Phys. 83:339 (2005).
- 66. Fernandes L, Antognini A, Boucher M, Conde C, Huot O, et al., Nucl. Inst. Meth. A 498:362 (2003).
- 67. Ludhova L, Amaro FD, Antognini A, Biraben F, Cardoso JMR, et al., Nucl. Inst. Meth. A 540:169 (2005).
- 68. Nebel T, Amaro FD, Antognini A, Biraben F, Cardoso JMR, et al., Can. J. Phys. 85:469 (2007).
- 69. Jentschura UD, Ann. Phys. 326:516 (2011).
- 70. Karr JP, Hilico L, Phys. Rev. Lett. 109:103401 (2012), [arXiv:1205.0633 (physics.atom-ph)].
- 71. Froelich P, Wallenius J, Phys. Rev. Lett. 75:2108 (1995).
- 72. Lindroth E, Wallenius J, Jonsell S, Phys. Rev. A 68:032502 (2003), Erratum Phys. Rev. A 69:059903(E) (2004).
- 73. Kilic S, Karr JP, Hilico L, Phys. Rev. A 70:042506 (2004).
- 74. Borie E, Rinker GA, Rev. Mod. Phys. 54:67 (1982).
- 75. Borie E, Phys. Rev. A 71:032508 (2005).
- 76. Borie E, Ann. Phys. 327:733 (2012), and arXiv: 1103.1772-v6.
- 77. Indelicato P, arXiv 1210.5828v2 (physics.atom-ph).
- 78. Carroll JD, Thomas AW, Rafelski J, Miller GA, Phys. Rev. A 84:012506 (2011).
- 79. Antognini A, Kottmann F, Biraben F, Indelicato P, Nez F, Pohl R,

- Ann. Phys. 331:127 (2013), arXiv:1208.2637.
80. Bethe HA, Salpeter EE, *Quantum Mechanics of One and Two Electron Atoms* (Springer (1957), Berlin, 1957).
81. Pachucki K, Phys. Rev. A 53:2092 (1996).
82. Kinoshita T, Nio M, Phys. Rev. Lett. 82:3240 (1999).
83. Ivanov VG, Korzinin EY, Karshenboim SG, Phys. Rev. D 80:027702 (2009).
84. Karshenboim SG, Korzinin EY, Ivanov VG, Shelyuto VA, JETP Lett. 92:8 (2010).
85. Friar J, Martorell J, Sprung D, Phys. Rev. A 59:4061 (1999).
86. Jentschura UD, Phys. Rev. A 84:012505 (2011).
87. Karshenboim SG, Ivanov VG, Korzinin EY, Phys. Rev. A 85:032509 (2012).
88. Jentschura UD, Ann. Phys. 326:500 (2011).
89. Martynenko AP, Physics of Atomic Nuclei 71:125 (2008).
90. Pachucki K, Phys. Rev. A 60:3593 (1999).
91. Carlson CE, Vanderhaeghen M, Phys. Rev. A 84:020102 (2011).
92. Hill RJ, Paz G, Phys. Rev. Lett. 107:160402 (2011).
93. Martynenko AP, Physics of Atomic Nuclei 69:1309 (2006), [arXiv: hep-ph/0509236].
94. Birse MC, McGovern JA, Eur. Phys. J. A 48:120 (2012), [arXiv: 1206.3030 (hep-ph)].
95. Miller GA, Thomas AW, Carroll JD, Rafelski J, Phys. Rev. A 84:020101 (2011), 1101.4073.
96. Miller GA, Thomas AW, Carroll JD, Phys. Rev. C 86:065201 (2012), 1207.0549.
97. Miller GA, Phys.Lett. B718:1078 (2012), 1209.4667.

- 98. Jentschura UD, Czarnecki A, Pachucki K, Phys.Rev. A 72:062102 (2005).
- 99. Jentschura UD, Mohr PJ, Phys.Rev. A 69:064103 (2004).
- 100. Yerokhin VA, Eur. Phys. J. 58:57 (2010).
- 101. Pachucki K, Jentschura UD, Phys. Rev. Lett. 91:113005 (2003).
- 102. Melnikov K, van Ritbergen T, Phys. Rev. Lett. 84:1673 (2000).
- 103. Eides MI, Shelyuto VA, Can. J. Phys. 85:509 (2007).
- 104. Shabaev VM, Teor. Mat. Fiz. 63:394 (1985).
- 105. Pachucki K, Grotch H, Phys. Rev. A 51:1854 (1995).
- 106. Eides MI, Grotch H, Phys. Rev. A 55:3351 (1997).
- 107. Shabaev VM, Artemyev AN, Beier T, Soff G, J. Phys. B 31:L337 (1998).
- 108. Pachucki K, Phys. Rev. A 52:1079 (1995).
- 109. Eides MI, Grotch H, Phys. Rev. A 52:1757 (1995).
- 110. Hertzog D, Morse W, Ann.Rev.Nucl.Part.Sci. 54:141 (2004).
- 111. Muon G-2 Collaboration, Bennett G, et al., Phys. Rev. D 73:072003 (2006),
hep-ex/0602035.
- 112. Jegerlehner F, Nyffeler A, Phys. Rep. 477:1 (2009), 0902.3360.
- 113. Fayet P, Phys. Rev. D 70:023514 (2004), hep-ph/0403226.
- 114. Finkbeiner DP, Weiner N, Phys. Rev. D 76:083519 (2007), astro-ph/0702587.
- 115. Pospelov M, Ritz A, Voloshin MB, Phys.Lett. B662:53 (2008), 0711.4866.
- 116. Barger V, Chiang CW, Keung WY, Marfatia D, Phys. Rev. Lett. 106:153001 (2011).
- 117. Barger V, Chiang CW, Keung WY, Marfatia D, Phys. Rev. Lett. 108:081802 (2012).
- 118. BABAR Collaboration, Aubert B, et al., Phys. Rev. Lett. 103:081803

- (2009), 0905.4539.
119. Wilczek F, Phys. Rev. Lett. 39:1304 (1977).
120. BABAR Collaboration, del Amo Sanchez P, et al., Phys. Rev. Lett. 104:191801 (2010), 1002.4358.
121. Barbieri R, Ericson TEO, Phys.Lett. B57:270 (1975).
122. Schmiedmayer J, Riehs P, Harvey JA, Hill NW, Phys. Rev. Lett. 66:1015 (1991).
123. Leeb H, Schmiedmayer J, Phys. Rev. Lett. 68:1472 (1992).
124. CLEO Collaboration, Insler J, et al., Phys. Rev. D 81:091101 (2010), 1003.0417.
125. NOMAD Collaboration, Altegoer J, et al., Phys.Lett. B428:197 (1998), hep-ex/9804003.
126. BES Collaboration, Ablikim M, et al., Phys. Rev. Lett. 97:202002 (2006), hep-ex/0607006.
127. Brax P, Burrage C, Phys. Rev. D 83:035020 (2011).
128. Khoury J, Weltman A, Phys. Rev. D 69:044026 (2004), astro-ph/0309411.
129. Khoury J, Weltman A, Phys. Rev. Lett. 93:171104 (2004), astro-ph/0309300.
130. Nicolis A, Rattazzi R, Trincherini E, Phys. Rev. D 79:064036 (2009), 0811.2197.
131. Tucker-Smith D, Yavin I, Phys. Rev. D 83:101702 (2011).
132. Batell B, McKeen D, Pospelov M, Phys. Rev. Lett. 107:011803 (2011).
133. Carlson CE, Rislow BC, Phys. Rev. D 86:035013 (2012), [arXiv:1206.3587v2 (hep-ph)].
134. A. Gasparian *et al.*, Jefferson Lab Experiment 12-11-106, unpublished. See

- http://www.jlab.org/exp_prog/proposals/12/C12-11-106.pdf.
135. R. Gilman *et al.*, arXiv 1302.2160. Paul Scherrer Institut Experiment R12-01.1, see <http://www.physics.rutgers.edu/~rgilman/elasticmup/>.
136. Flowers JL, Baird PEG, Bougueroua L, Klein HA, Margolis HS, IEEE Trans. Instrum. Meas. 56:331 (2007).
137. Beyer A, Alnis J, Khabarova K, Matveev A, Parthey CG, et al., Ann. d. Phys. (Berlin) (2013), DOI 10.1002/andp.201300075.
138. Arnoult O, Nez F, Julien L, Biraben F, Eur. Phys. J. D 60:243 (2010).
139. Peters E, Diddams SA, Fendel P, Reinhardt S, Hänsch TW, Udem T, Opt. Expr.. 17:9183 (2009).
140. Herrmann M, Haas M, Jentschura U, Kottmann F, Leibfried D, et al., Phys. Rev. A 79:052505 (2009).
141. Kandula DZ, Gohle C, Pinkert TJ, Ubachs W, Eikema KSE, Phys. Rev. A 84:062512 (2011).
142. van Rooij R, Borbely JS, Simonet J, Hoogerland MD, Eikema KSE, et al., Science 333:196 (2011).
143. Sick I, Phys. Rev. C 77:041302 (2008).
144. Antognini A, Nez F, Amaro FD, Biraben F, Cardoso JMR, et al., Can. J. Phys. 89:47 (2010).
145. Tan JN, Brewer SM, Guise ND, Phys. Scr. T144:014009 (2011).
146. Vutha AC, Bezginov N, Ferchichi I, George MC, Isaac V, et al., Bull. Am. Phys. Soc. 57(5):Q1.138 (2012), <http://meetings.aps.org/Meeting/DAMOP12/Event/171433>.
147. Hagley EW, Pipkin FM, Phys. Rev. Lett. 72:1172 (1994).
148. Crivelli P, Cesar CL, Gendotti U, Can. J. Phys. 89:29 (2010).

149. Cassidy DB, Hisakado TH, Tom HWK, Mills AP, Phys. Rev. Lett. 109:073401 (2012).
150. Antognini A, Crivelli P, Prokscha T, Khaw KS, Barbiellini B, et al., Phys. Rev. Lett. 108:143401 (2012).
151. Pohl R, Amaro FD, Antognini A, Biraben F, Cardoso JMR, et al., Journal of Physics: Conference Series 264:012008 (2011), 22nd International Conference on Atomic Physics (ICAP 2010) Cairns, Australia, 25-30 July 2010.
152. Parthey CG, Matveev A, Alnis J, Pohl R, Udem T, et al., Phys. Rev. Lett. 104:233001 (2010).
153. Drake GWF, Byer LL, Phys. Rev. A 32:713 (1985).
154. Nörtershäuser W, Sánchez R, Ewald G, Dax A, Behr J, et al., Phys. Rev. A 83:012516 (2011).
155. Nörtershäuser W, Tiedemann D, Žáková M, Andjelkovic Z, Blaum K, et al., Phys. Rev. Lett. 102:062503 (2009).
156. Krieger A, Blaum K, Bissell ML, Frömmgen N, Geppert C, et al., Phys. Rev. Lett. 108:142501 (2012).

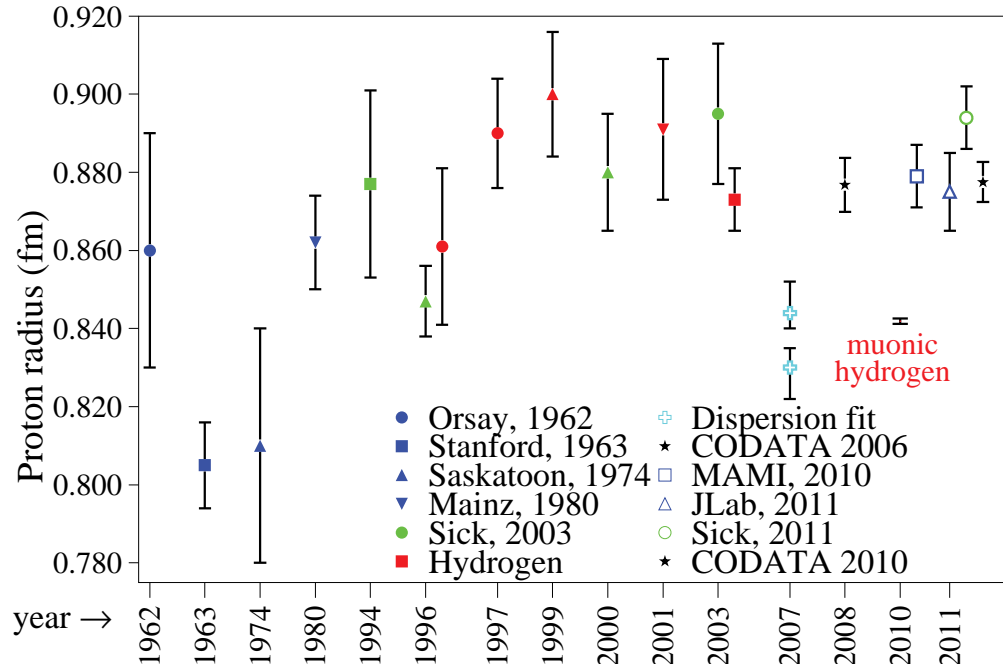


Figure 1: Proton radius determinations over time. Electronic measurements seem to settle around $r_p=0.88$ fm, whereas the muonic hydrogen value [1,2] is at 0.84 fm. Values are (from left to right): Orsay [10], Stanford [11], Saskatoon [12, 13], Mainz [14] (all in blue) are early electron scattering measurements. Recent new scattering measurements are from MAMI [4] and Jlab [15]. The green and cyan points denote various reanalyses of the world electron scattering data [16–21]. The red symbols originate from laser spectroscopy of atomic hydrogen and advances in hydrogen QED theory (see [3] and references therein). The green and red points in the year 2003 denote the reanalysis of the world electron scattering data [19] and the world data from hydrogen and deuterium spectroscopy which have determined the value of r_p in the CODATA adjustments [3, 22] since the 2002 edition.

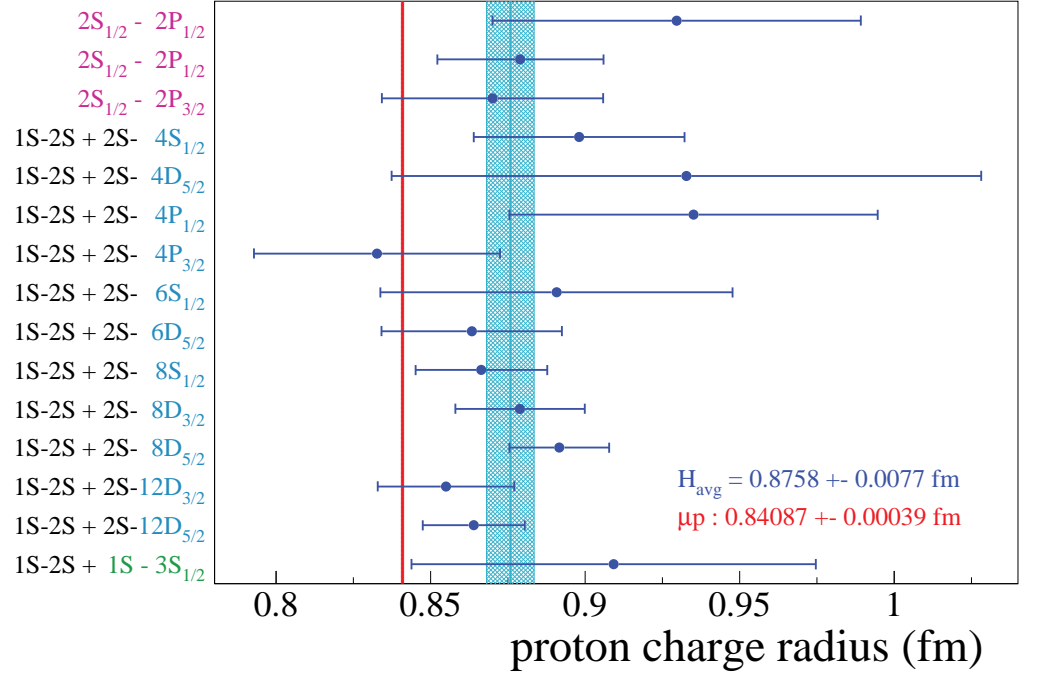


Figure 2: Proton charge radii r_p obtained from hydrogen spectroscopy. According to Eq. (4), r_p can best be extracted from a combination of the 1S-2S transition frequency [25] and one of the 2S-8S,D or 12D transitions [26,27]. The value from muonic hydrogen [1,2] is shown with its error bar.

Table 1: Numerical results for the $\mathcal{O}(\alpha^5)m^4$ proton structure corrections to the Lamb shift in muonic hydrogen. Energies are in μeV .

(μeV)	Ref [91]	Ref. [81, 90]	Ref. [93]
ΔE^{subt}	5.3 ± 1.9	1.8	2.3
ΔE^{inel}	-12.7 ± 0.5	-13.9	-16.1
ΔE^{el}	-29.5 ± 1.3	-23.0	-23.0
ΔE	-36.9 ± 2.4	-35.1	-36.8

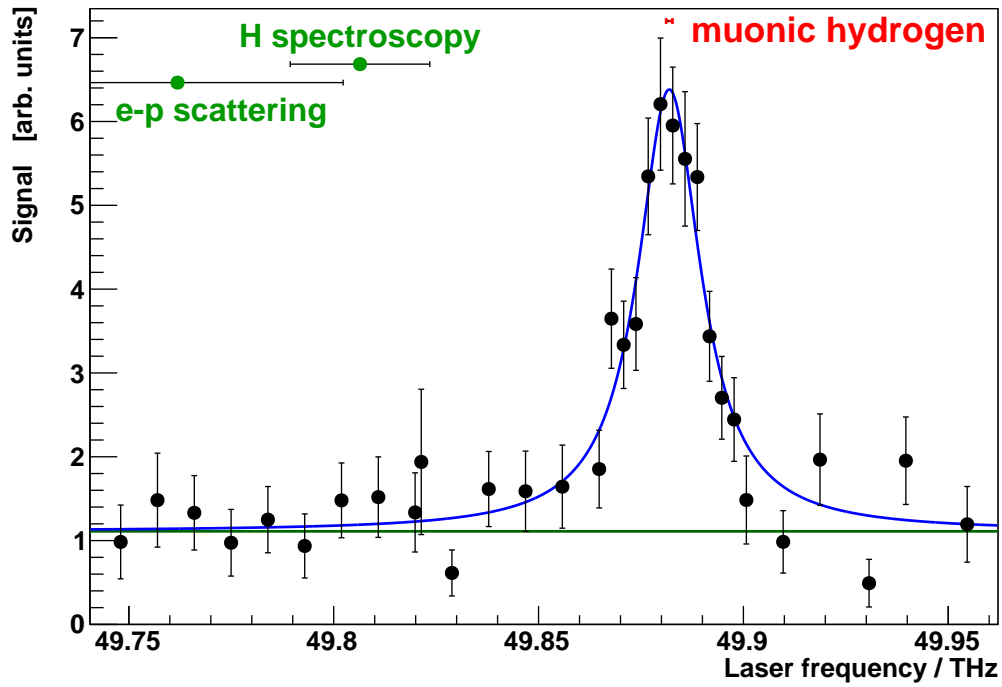


Figure 3: Resonance in muonic hydrogen, together with the positions predicted using the proton radii from elastic electron-proton scattering using pre-2009 world data [19, 23] and the CODATA-2006 value from H spectroscopy [22].

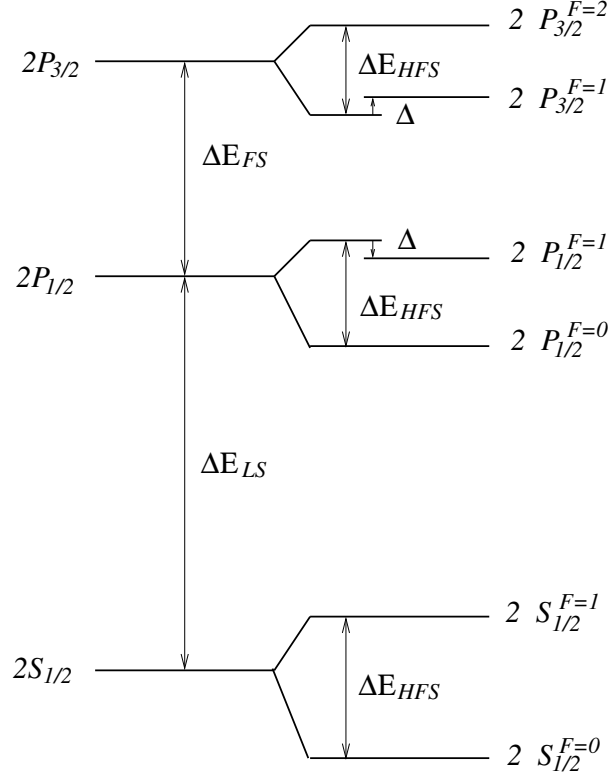


Figure 4: Level scheme of muonic hydrogen for $n = 2$ shell, the artificial $2P_{1/2}$ and $2P_{3/2}$ levels corresponds to centroid for $\Delta = 0$. Numerical values for level splittings are presented in Eq. (32).

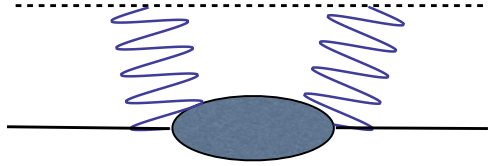


Figure 5: The box diagram for the $\mathcal{O}(\alpha^5 m^4)$ corrections. The graph in which the photons cross is also included in the calculation. The blob represents all possible excitations of the proton, the wiggly lines represent the exchanged photons. The solid line represents the proton and the dashed line represents the muon.